



universität  
wien

# MASTERARBEIT / MASTER'S THESIS

Titel der Masterarbeit / Title of the Master's Thesis

„Novel 3D-printed cell culture inserts for  
advanced *in vitro* skin regeneration“

verfasst von / submitted by

Magdalena Bauer, BSc

angestrebter akademischer Grad / in partial fulfilment of the requirements for the  
degree of

Master of Science (MSc)

Wien, 2021 / Vienna, 2021

Studienkennzahl lt. Studienblatt /  
degree programme code as it appears on  
the student record sheet:

UA 066 834

Studienrichtung lt. Studienblatt /  
degree programme as it appears on  
the student record sheet:

Masterstudium Molekulare Biologie

Betreut von / Supervisor:

Univ. Prof. Dr. Johannes Grillari



## Abstract

In skin research, 2D monolayer *in vitro* models provide only limited fields of application as they do not sufficiently mimic physiological properties, like functional skin barrier (SB). Since in the spirit of 3R's (Replacement, Reduction, and Refinement) animal models are to be avoided, new approaches like 3D skin equivalents (SE) are needed to close the *in vitro/in vivo* gap. Cell culture inserts for the production of SE are commercially available, however, these inserts are expensive and limited regarding the experimental setup. This work aimed to establish and evaluate novel lab-based 3D printed cell culture inserts for full thickness SE generation. A computer-aided design model was realized with extrusion-based 3D printing of polylactic acid (PLA) filament. While improving the insert, we went through six construction versions. PLA printing material was evaluated regarding cytotoxicity according to ISO 10993-5 and nanoparticle analysis. No objections were found. In a next step, a full thickness SE was created on a collagen/fibrin dermal scaffold. Cell culture experiments successfully demonstrate that it is technically possible to generate SE on the in-house inserts. SB was tested by performing skin permeability assays. Here, the diffusion of fluorescent dyes was quantified. First measurements using Riboflavin and Alexa Flour® indicate the very good performance of the 3D printed system. This work provides valuable know-how for the generation of SE, as well as testing the SB in-house. The system is accessible to everyone with a 3D printer, variable in printing material, compatible to commonly used cell culture plates, very cost-effective and easy to handle.

**Keywords:** Skin equivalents; 3D printing; full thickness skin model; insert; skin barrier; skin permeability assay; cytotoxicity

## Zusammenfassung

Unsere Haut ist das größte und eines der komplexesten Organe des menschlichen Körpers. Da 2D Monolayer Kulturen stark vom physiologischen Verhalten abweichen, werden häufig Tiermodelle eingesetzt, um die Funktion gesunder und kranker menschlicher Haut zu untersuchen. Im Sinne der 3Rs (Replacement, Reduction, und Refinement) werden 3D Hautequivalente genutzt, um die Lücke zwischen Tiermodell und Monolayer Kultur zu schließen. Diese Hautäquivalente werden entweder teuer gekauft oder selbst im Labor auf gekauften Inserts gezüchtet. Ziel dieser Arbeit ist es, solche Inserts mittels 3D Druck herzustellen, um in ihnen „full thickness“ Hautäquivalente zu züchten und die Hautbarrierefunktion zu testen. Dazu wurde ein computergestütztes Designmodell erstellt und mittels extrusionsbasiertem 3D Druck von Polymilchsäure (PLA) Filament realisiert. Das PLA wurde hinsichtlich Zytotoxizität gemäß ISO 10993-5 bewertet. Weiteres wurden „full thickness“ Hautäquivalente mit einer humanen Fibroblastenzelllinie und humanen epidermalen Hautkeratinozyten auf einem Kollagen/Fibrin Gel hergestellt. Um die Hautbarriere zu untersuchen, wurde eine quantitative Fluoreszenzmessung von Fluoreszenzfarbstoffen durchgeführt. Von der initialen Konstruktion, bis zur finalen funktionstüchtigen Version wurden sechs Konstruktionsvarianten durchlaufen. Zellkulturexperimente zeigten erfolgreich, dass es technisch möglich war, „full thickness“ Hautäquivalente auf den hauseigenen 3D gedruckten Inserts zu erzeugen. PLA zeigte in der MTT-Analyse keine Anzeichen für Zytotoxizität. Hautbarrierefunktionuntersuchungen mittels Fluoreszenzmessungen von Riboflavin und Alexa Flour® gaben erste Hinweise für die Verwendbarkeit des 3D gedruckten Systems. Mit dieser Arbeit wird ein Puzzlestück zur Verfügbarkeit von 3D Hautmodellen in Forschungslaboren hinzugefügt. Das System ist variabel in Druckmaterial, Membranmaterial sowie in der Größe. Darüber hinaus ist es mit gängigen Zellkulturplatten kompatibel, kostengünstig und einfach in der Handhabung.

**Schlagwörter:** Hautäquivalente; 3D Druck; „full thickness“ Hautäquivalente; Inserts; Hautbarriere; Hautbarrierefunktionuntersuchung; Zytotoxizität

## Acknowledgements

I want to thank my supervisor Assoc. Prof. Dr. Johannes Grillari for giving me the opportunity to implement my master thesis at the Ludwig Boltzmann Institute for experimental and clinical traumatology and supporting me throughout the process. Next, I want to deeply thank Peter Dungal, for always being open towards my ideas, answering my questions, for his patience and all the opportunities he provided. Further, I would like to express my gratitude to Magdalena Metzger, who trained me and from whom I not only received amounts of knowledge, but who also invested a lot of her own time into this thesis.

I would like to express a very special thank you to Marvin Corea, who not only supported me with his technical skills, but also with his encouraging and optimistic nature in all phases of the thesis.

Additionally, I also want to thank all my colleagues from the LBI Trauma, in particular Carina Wagner, Jaana Hartmann, Stefan Manhartseider and Johannes Oesterreicher. They are such kind and welcoming people, who are always supportive and answered my questions when needed. I appreciate our friendships, when discussing work or personal matters with you and celebrating each other's successes.

I am also deeply grateful for the continuous support from my family throughout my studies, they fill my life with love and joy!

And to say it in Snoop Doggs words:

*“Last but not least, I wanna thank me. I wanna thank me for believing in me, I wanna thank me for doing all this hard work”*

# Table of Contents

1	Introduction .....	6
1.1	Skin anatomy .....	6
1.2	Skin barrier .....	8
1.3	Artificial skin / Skin equivalents .....	9
1.3.1	Necessity of skin equivalents .....	9
1.3.2	History of in vitro 3D skin models .....	10
1.4	3D Printing .....	11
1.4.1	Extrusion based 3D printing technique .....	12
1.4.2	Printing material .....	12
1.5	Project Aim .....	13
2	Material and Methods.....	14
2.1	Construction and printing of inserts .....	14
2.2	Cell Culture .....	15
2.3	Cytotoxicity assay according to ISO 10993-5.....	15
2.4	Nanoparticle tracking analysis .....	18
2.5	Generation of skin equivalents .....	18
2.6	Histology .....	19
2.7	Permeability assay .....	20
2.8	Statistics .....	20
3	Results .....	21
3.1	Construction of inserts .....	21

3.2	Excursion twist lock .....	27
3.3	Permeability ring .....	27
3.4	Evaluation of printing material.....	29
3.4.1	Evaluation of cytotoxicity .....	29
3.4.2	Nanoparticle tracking analysis.....	29
3.5	Generation of full thickness skin equivalents.....	30
3.5.1	Pilot trails of 3D printed vs. commercial inserts .....	30
3.5.2	Media condition testing .....	32
3.5.3	Refinement of skin equivalent generation procedure .....	34
3.5.4	Establishment of skin barrier assay .....	36
4	Discussion.....	38

# 1 Introduction

## 1.1 Skin anatomy

With a total area of 1.7 m<sup>2</sup> and weighing in at 15 % of the body mass the skin is the largest and one of the most complex human organs. It provides a protective barrier against environmental exposures. It shields the inner tissues and organs from outer noxae, including mechanical stress, radiation, microbial infection, and extreme temperatures. The integrity of the skin plays an essential role in the maintenance of physiological homeostasis. Structures like hair, glands and nails are formed by or harboured within the skin.

Human skin structure (Figure 1) can be divided into *epidermis*, *dermis*, and *hypodermis* [1,2].

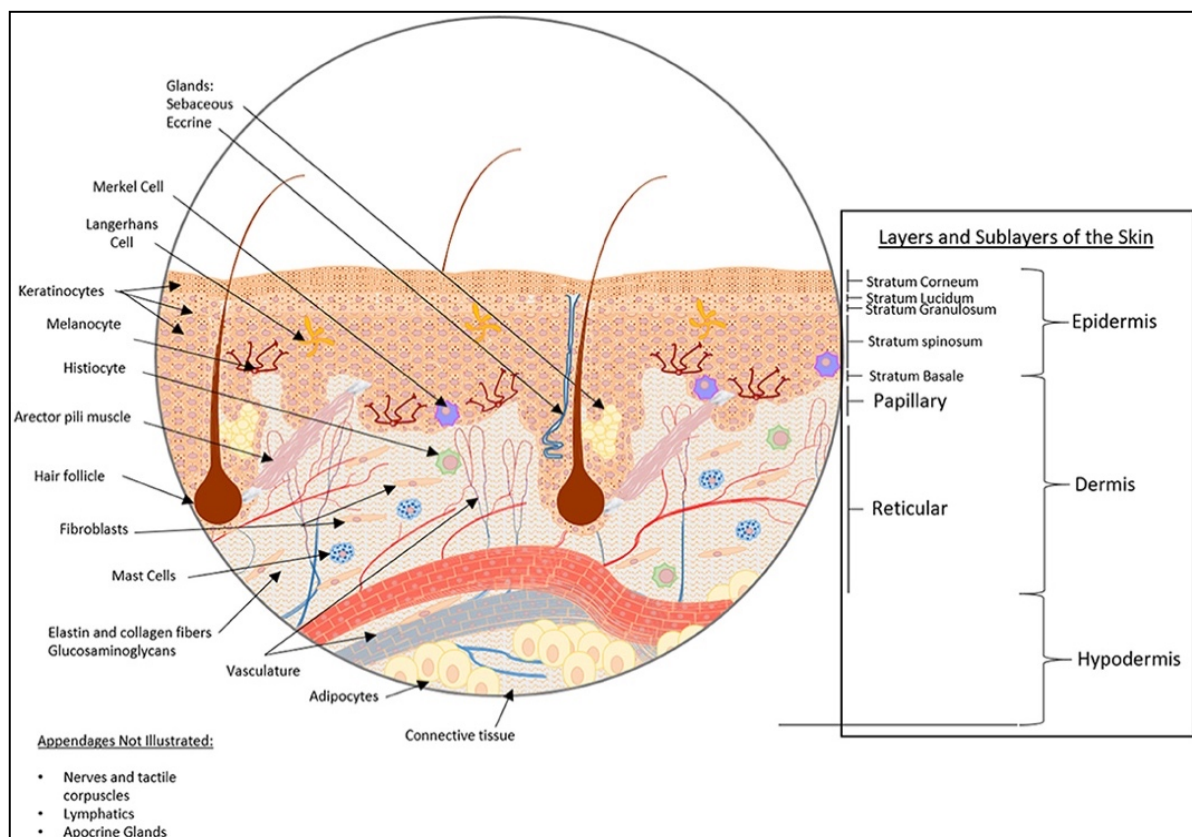


**Figure 1 Skin structure** showing the epidermal, dermal, and hypodermal layers and their sublayers. The epidermis is divided into *stratum corneum*, *lucidum*, *granulosum*, *spinosum* and *basale*. The dermis is subdivided into the *papillary* and *reticular layer*. Moreover, cell types of the skin include: keratinocytes, Merkel cells, Langerhans cells, melanocytes, histiocytes, fibroblasts, mast cells, and adipocytes are represented. Skin appendages, like hair and glands are also shown. Taken from [3]

The avascular *epidermis* is the skin's most superficial layer that is stratified into sublayers. Its structure is depicted in **Figure 2**. A single layer, mostly made up from basal cells, which are the precursors of keratinocytes, forms its base, the *stratum basale*. It also harbours Merkel cells and melanocytes. The basal cells are constantly dividing, thereby producing new keratinocytes that push the older ones further upwards, away from the *stratum basale*, towards the *stratum corneum*. The *stratum corneum* is the most superficial layer of the epidermis. It is dry and consist of 15-30 layers of dead, cornified keratinocytes. This thick and robust layer prevents the incursion of pathogens and protects the underlying layers from dehydration and mechanical stress from the outside environment. Due to the constant replenishment and ascension of the cells from the *stratum basale*, the entire *stratum corneum* is renewed every 4 weeks [1].

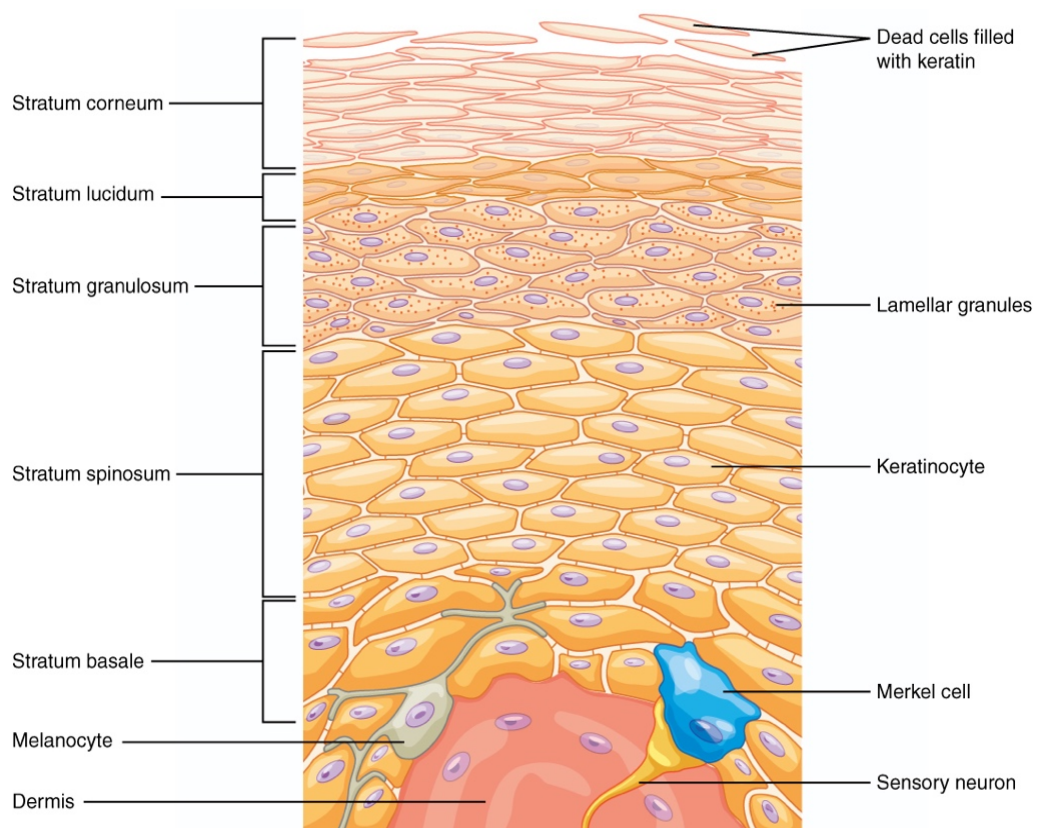


**Figure 2 Layers of the epidermis.** The epidermis is divided into *stratum corneum*, *lucidum*, *granulosum*, *spinosum* and *basale* (top to bottom). The dermis is implied next to the *stratum basale* harbouring a sensory neuron. Also, a melanocyte and a Merkel cell is represented. The alteration of keratinocytes on their way from the *stratum basale* to the *stratum corneum* is shown here as keratinocytes that turn into cells with lamellar granulae and furthermore into dead cells filled with keratin. Taken from [1]

On their way from the *stratum basale* to the *stratum corneum*, the skin cells undergo distinctive phases of development, which define the three intermediary layers of the epidermis. The *stratum spinosum* lies above the *stratum basale*, that is composed of eight to ten layers of keratinocytes, which are defined by the synthesis of keratin. Amongst the keratinocytes, macrophages called Langerhans cells are dispersed. In the continuous process of keratinocyte production in the *stratum basale*, the older keratinocytes are pushed upwards by younger ones into the *stratum granulosum*. There, due to losing their nucleus, cells take on a flatter shape with thicker cell membranes. The increased production of keratin and keratohyalin forms lamellar granules within the cells. In body regions which are exposed to tear and wear, such as the palms of the hands or the soles, a fifth layer, called *stratum lucidum* is formed as an additional protective layer [3,4].

The *dermis* is located under the epidermis and consists of two layers of connective tissue, which contain blood vessels, lymphatic vessels, nerves, hair follicles and sweat glands. The main function of the dermis is to maintain the hydration of the skin. It harbours connective tissue out of an interconnected mesh of elastin and collagenous fibres, produced by fibroblasts. The upper layer is the *papillary layer*, which is thinner, composed out of loose connective tissue and connects the epidermis with the dermis. The deeper layer is the thicker *reticular layer*, comprised of dense connective tissue out of collagen fibres with less cells/fibroblasts in it. This layer makes up approximately 80 % of the dermis [1,4].

The *hypodermis* (also called subcutaneous fascia) is the deepest layer of the skin and is the connection of the skin to the underlying fibrous tissue, that surrounds the muscles. Its main function is to isolate and cushion the body, which is achieved by storing fat in adipocytes [1].

## 1.2 Skin barrier

The skin forms the protective layer of the body which separates the organism from the environment. Without this protective barrier incursion of noxae, such as viruses, bacteria [5], but also physical stresses would quickly lead to the organism's demise [6]. It does however not only prevent external damage but also damage caused by the loss of internal substances, e.g. the rapid loss of fluid and electrolytes in burn victims, when a significant portion of the body surface area has been destroyed [7]. Moreover, many skin disorders are associated with impaired skin barrier function, such as atopic dermatitis [8] and psoriasis.

Atopic dermatitis is a chronic, inflammatory, and eczematous skin disease, caused by filaggrin protein deficiency, climate, air pollution, food allergies, and obesity [9]. In Germany 10.35 % of all children [10] and 3.65 % of all adults [11] are affected. Psoriasis genetic skin disease, which is associated with both a physical and psychological burden to the patients [12]. The prevalence in German population is 3.8 %. Topical therapy is the most common therapeutic option applied in 42.4 % of all investigated psoriasis patients [13] and plays a major role in the therapy of atopic dermatitis as well [14]. The treatment of burn wounds also includes topic creams, dressings and solutions in the acute, as well as the rehabilitation phase in order to create a physical barrier and administer drugs [15]. The testing of these agents is imperative. In the following chapters, the importance of model systems, especially *in vitro* models are described.

## **1.3 Artificial skin / Skin equivalents**

### **1.3.1 Necessity of skin equivalents**

Human skin models are important tools for research, clinical purposes, and industrial applications. Animal models are often used for this in the area of skin research [16], as 2D monolayer *in vitro* models lack cell–cell and cell–matrix interactions and do not exhibit physiological behaviour, like functional skin barrier properties. Such, 2D models allow only very limited inference about physiological responses of organisms to external stimuli. *In vivo* models can provide that complex information, however, but there has been a general concern for the animal suffering experienced during research. This is what inspired W. Russell and R. Burch to write and publish a guide to maximally reduce animal pain in 1959 [17]. There they established the principles of the three R's: Replacement, Reduction, and Refinement. Today the 3R's are fixed in legislation regulating the use of animals for scientific studies, like the Directive 2010/63/EU [18] for the European Union.

In an attempt to close the *in vitro*–*in vivo* gap, there is a high demand for novel *in vitro* model systems that mimic closely the human skin and forecast physiological behaviour of healthy and diseased skin tissue.

### 1.3.2 History of *in vitro* 3D skin models

First steps of the generation of skin equivalents (SE) took place in 1951, when the first method to separate the epidermis from the dermis, followed by isolation and culturing of human keratinocytes was described [19]. A few years later, in 1957, it was demonstrated that cells obtained from human epidermis biopsies can undergo long-term culture [20]. Rheinwald and Green achieved a huge milestone in 1975 by culturing single human keratinocytes on a feeder layer of lethally irradiated 3T3 fibroblasts, where, single keratinocytes generated colonies [21]. This knowledge was the basis for the *in vitro* culturing of keratinocytes in high quantities [22], as well as the creation of autologous epithelial grafts for transplantation onto burn wounds in humans [23]. One of the first explant 3D models was described in 1976, where Freeman et al. showed that keratinocytes undergo maturation into distinct basal, squamous, granular, and keratinized cell layers. The group cultured human keratinocytes onto inverted sterile dead pig skin. As the cells grew, they digested the dermal collagen of the inverted pig skin [24]. Later, this method was improved by using collagen as a dermal substitute to successfully culture keratinocytes at the air-liquid interface (ALI). With this method, the culture medium does not completely cover the graft. The surface of the liquid stands at the border between the top layer of cells and air. Culturing the cells on the ALI enhanced the degree of tissue organization and differentiation [25]. Another major milestone was achieved in the 1980s where the group around E. Bell managed to incorporate fibroblasts into the collagen [26] in order to later produce the first "full thickness" skin model, which was successfully transplanted onto rats [27]. The full thickness model reconstructed the dermis and the epidermal skin layer. This model was also used in the present work. In addition to the full thickness model, other models were established in the 1980s. In **Figure 3**, a rough overview of the types of equivalents is depicted.

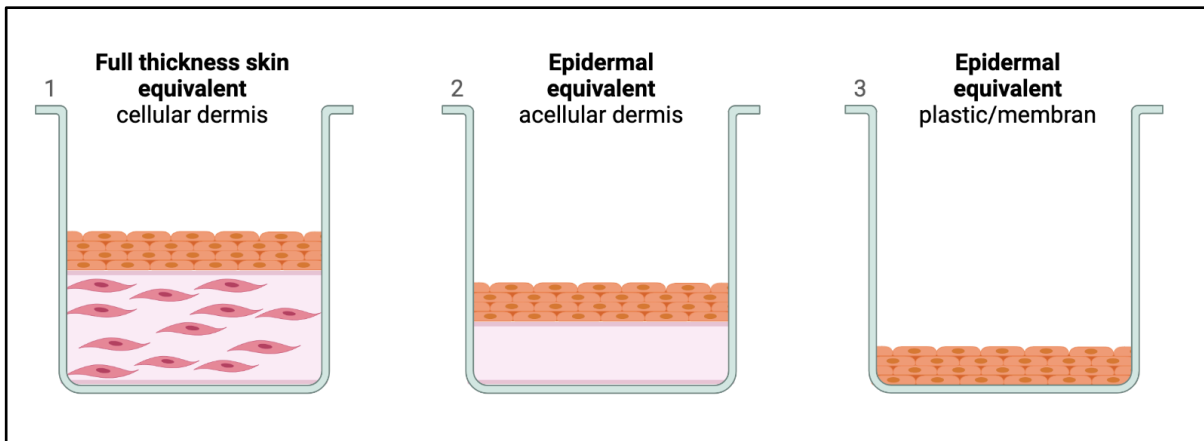


**Figure 3 Types of skin equivalents.** To build 3D skin models keratinocytes can be grown on: (1) a cellular matrix (collagen-fibroblast matrix), (2) an acellular matrix (gel or de-epidermized dermis) or (3) on plasticware or various membranes. After cultivation for several days, the culture medium level is lowered in order to grow the skin equivalents at the air-liquid interface. Days to weeks later, a multilayered stratified epidermis is formed. Created with BioRender.com.

In current literature various forms of the full thickness skin and the epidermal equivalents are described, harbouring amongst others: melanocytes [28], immune cells [29] or endothelial cells [30]. Meanwhile, human SE can also be purchased commercially. There are several different providers who sell their products to a wide variety of institutions. This includes various companies with a wide range of products, such as SkinEthic™ [31] and EpiSkin™ (Episkin SNC, France), EpiDerm™ (MatTek, USA) [32] or Phenion® (Phenion, Germany). However, these commercially available products are cost-intensive, limited in size, and often have long transport routes that involve delivery times. An alternative to this are lab-made, in-house SEs.

## 1.4 3D Printing

The relatively novel technique of three-dimensional (3D) printing has several advantages compared to conventional manufacturing processes, such as increased quality, cost-effectiveness and higher efficiency and thus has impacted several biomedical engineering applications, including surgical guides, tissue regeneration, artificial scaffolds, and implants, as well as the administration and delivery of drugs [33].

The American Society for Testing and Materials (ASTM) classifies 3D printing technologies in seven main categories: binder jetting (e.g., 3D printers that utilize binder and powder); directed energy deposition (e.g., laser cladding); material extrusion (e.g., fused deposition

modelling); material jetting (e.g., Polyjet); powder bed fusion (e.g., selective laser sintering); sheet lamination (e.g., sheet forming); vat polymerization (e.g., stereolithography) [34].

#### **1.4.1 Extrusion based 3D printing technique**

Extrusion-based 3D printing is one of the most common printing methodologies, and was used in this present study – specifically, a method called fused deposition modelling (FDM) or fused layer modelling (FLM). It is described in the following:

First, extrusion-based 3D printing processes require a digital computer-aided design model (CAD), which is then sliced into single layers. These layers are used to derive the path that the printer nozzle has to travel in order to create a 3D model of the construction. The printing materials, also called filaments are thermoplastic polymers. The filament is rolled up like a thread on a roll and ends in a heat chamber. A pinion with a stepper motor is used to feed the filament to the heat chamber. The material is melted in the heat chamber and pressed into the nozzle by the filament that follows. The nozzle is located behind the heat chamber and moves over the printing platform during the printing process. The extruded material is deposited layer-by-layer and a printing platform moves on the y axes, while the stage moves in x and z directions which allows the production of versatile 3D objects with modulable shapes and dimensions. Depending on the specific printer models, the traverse paths of the axes can differ. The most used polymers are polylactic acid- (PLA) and acrylonitrilebutadiene-styrene (ABS)-based filaments [34,35].

#### **1.4.2 Printing material**

For this work PLA was used as filament. PLA is a common material, which is the most extensively studied aliphatic polyester. It is the top 3D printing industry leading biomaterial in replacing petrochemical based polymers [37], derived 100 % from renewable resources. PLA is highly versatile, biodegradable, biocompatible and has suitable mechanical properties, like thermoplastic processibility [38]. The educt of PLA is lactic acid, which is a naturally occurring organic acid that can be produced by fermentation of sugars obtained from renewable resources such as sugarcane. When hydrolytically degraded, PLA converts back to lactic acid [39]. PLA has extensive applications in the biomedical field.

## 1.5 Project Aim

This study aimed to develop and manufacture 3D printed more sustainable, cost-effective, faster producible, and convenient cell culture inserts for the generation of full thickness skin equivalents (Figure 4). Further, to test the feasibility in terms of handling, cell growth, cytotoxicity, and functionality, by the extension of a permeability assay.

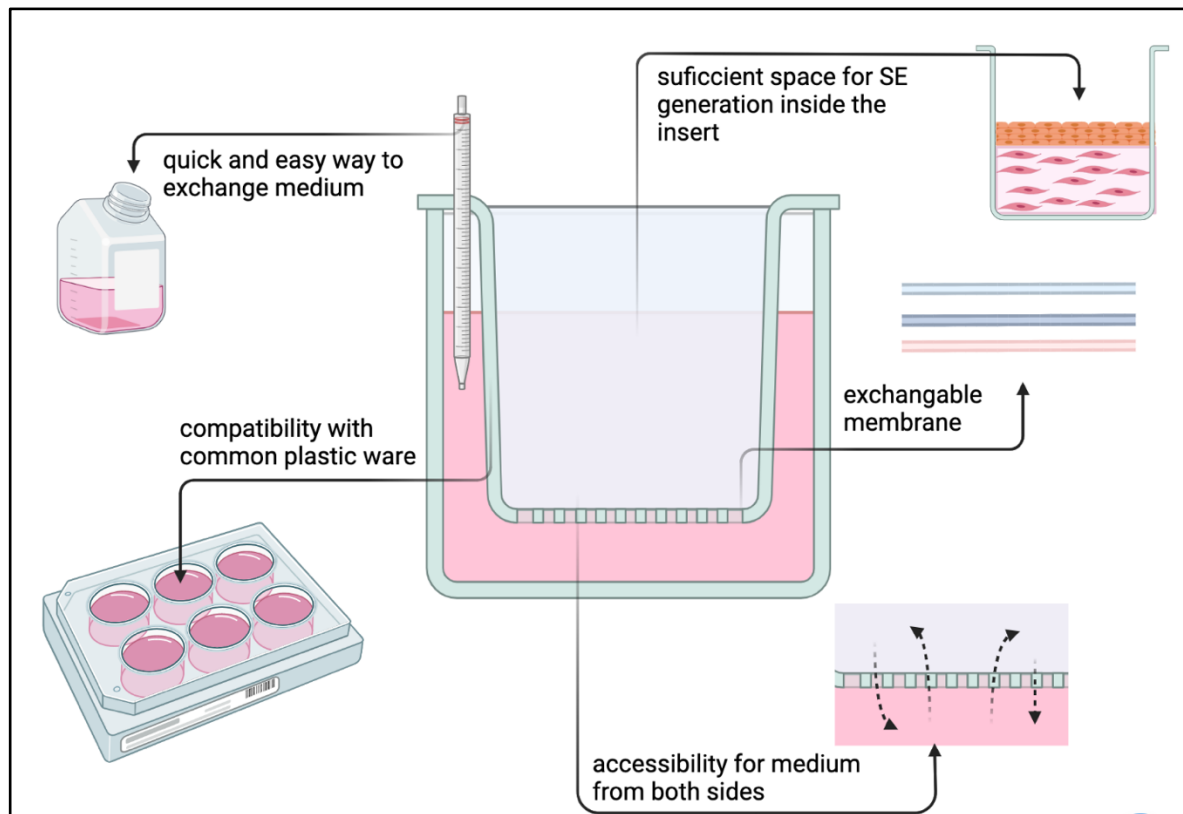


**Figure 4 Requirements for cell culture inserts:** a practical way to exchange media; sufficient space within the insert for the volume, that is required for the generation of SE; possibility to use different membrane materials; hanging membrane to enable nutrient exchange trough both sides of the membrane, compatibility with common cell culture plastic ware. Created with BioRender.com.

## 2 Material and Methods

### 2.1 Construction and printing of inserts

The CAD model was constructed using Solidworks 2021 software (Dassault Systèmes, France). For the printing an Ender 3 Pro (Shenzhen Creality 3D technology, China) printer was utilized. All inserts were printed with PLA (Shenzhen Getech Technology, China) of transparent colour. Printing parameters were tested by trial and error, changing fill density, printing temperature, printing speed, retraction, and retraction speed. The final printing parameters are shown in **Table 1**. With these parameters stringing was avoided, and the result was an even print image.

**Table 1 Final printing parameters.** In the columns the parameter name, the associated units and final values are listed.

Parameters	Unit	Value
Layer height	mm	0.2
Nozzle outlet	mm	0.4
Wall thickness	mm	0.8
Fill density	%	100
Printing temperature	°C	205
Printing plate temperature	°C	60
Printing speed	mm/s	50
Moving speed	mm/s	100
Retraction	mm	6.5
Retraction speed	mm/s	33
Printing plate adhesion type	/	skirt

To create the rendered graphics of the constructs Solidworks photoView 360 software (Dassault Systèmes, France) was used.

To stylize the 3D printed inserts for cell culture use, the devices were submersed in 70 % ethanol for at least 15 min. To assemble the inserts, the Nucleopore Track-Etch membrane (Whatman, UK) with 3  $\mu$ m pores was placed between the dried lower part and the upper

section of the device. Subsequently the assembled insert was placed on top of a plastic lid in the laminar flow hood and irradiated for at least 15 min with ultraviolet (UV) light. After the irradiation, the inserts were placed – depending on insert size – into 6-well or 12-well plates (CoStar Group, USA).

## **2.2 Cell Culture**

For all experiments, a human dermal fibroblast cell line (fHDF/TERT166, Evercyte, Austria) and normal human epidermal skin keratinocytes (NHEK/SVTERT 3-5, Evercyte, Austria) were used. Cells were cultured at 37 °C, 5 % CO<sub>2</sub> and moderate humidity. Thawing of the fibroblasts and keratinocytes was conducted according to manufacturer's instructions.

Expansion of fibroblasts was performed in T175 flasks (Greiner Bio-One, Austria) with a 1:1 medium mixture of Dulbecco's Modified Eagle Medium (DMEM-high glucose containing phenol red, Sigma-Aldrich, USA) and Ham's F-12 (Lonza, Swiss) supplemented with 10 % FCS (Sigma-Aldrich, USA), 2 mM glutamine (GlutaMax, Gibco, USA) and 1 µg/ml G148 (InvitroGen, USA). When cells reached a confluency over 80-90 %, they were split in a ratio of 1:3 or 1:4. Cells were washed twice with PBS (Lonza, Swiss) before adding 2.5x Trypsin/EDTA (Sigma-Aldrich, USA) diluted 1:4 in PBS for 5 minutes at 37 °C. The reaction was stopped by adding double the amount of cell culture medium. Expansion of keratinocytes was also performed in T175 flasks with KBM-2 growth medium (Lonza, Swiss), supplemented with KGM-2 keratinocytes medium SingleQuote kit (Lonza, Swiss). To detach the cells, a 1:2 dilution of 2.5x Trypsin/EDTA in PBS was used after two washing steps with PBS. The reaction was stopped with equal the amount of trypsin neutralizing solution (Gibco, USA) and washed with 10 ml PBS. From this step onwards, the procedure was identical for both cell types. The cell suspensions were centrifuged at 100×g for 5 minutes in a 50 mL Falcon Tube (Greiner Bio-One, Austria). Cell pellets were resuspended in fresh medium and seeded into a T175 flask. In the case of subconfluency, cell culture medium was exchanged every third or fourth day.

## **2.3 Cytotoxicity assay according to ISO 10993-5**

Cytotoxic effects of transparent PLA material on keratinocytes and fibroblast in their respective medium was investigated following the ISO standard 10993-5. This standard offers the choice of different assays to determine cytotoxicity. We choose thiazolyl blue

tetrazolium bromide (MTT) assay and visible validation. The process is shown schematically in Figure 5.

Briefly, keratinocytes were seeded at a cell concentration of  $1 \cdot 10^5$  cells/ml, fibroblasts at  $1 \cdot 10^5$  cells/ml into a 96-well plate to reach a confluency of 50 % the next day. The first and the last were spared to avoid edge effects. Two columns were only filled with media for a non-cell control. 24 h after seeding 100  $\mu$ l treatment media was applied to the wells. Treatment medium was created by placing sterilized inserts into a 6-well plate (Corning, USA) filled with 4 ml keratinocytes or fibroblast growth medium respectively. Freshly printed, as well as used inserts were tested, and the results were compared to each other. The used inserts were stored in 70 % ethanol until use. Treatment medium was applied in concentrations ranging from 0-100 %. 0 % treatment media was equal to fresh cell culture medium, 50 % is a 1:1 mixture of fresh and 100 % medium, that was incubated with the insert. Cells were incubated for 24 h with treatment media groups. 25 mg of MTT powder (Thermo Fisher Scientific, USA) were dissolved in 5 mL sterile PBS to make a 5 mg/ml MTT stock solution. Next the treatment media were discarded. Then, 50  $\mu$ L of MTT stock solution were added to each well. After an incubation period of 2 h at 37 °C, the reagent was removed from each well. Afterwards, 100  $\mu$ L Isopropanol (Sigma-Aldrich, USA) were added and plates were incubated for 30 min on an orbital shaker (VWR International, USA). Absorbance was then measured at 570 nm (reference wavelength 650 nm) on a plate reader (BMG Labtech, Germany).

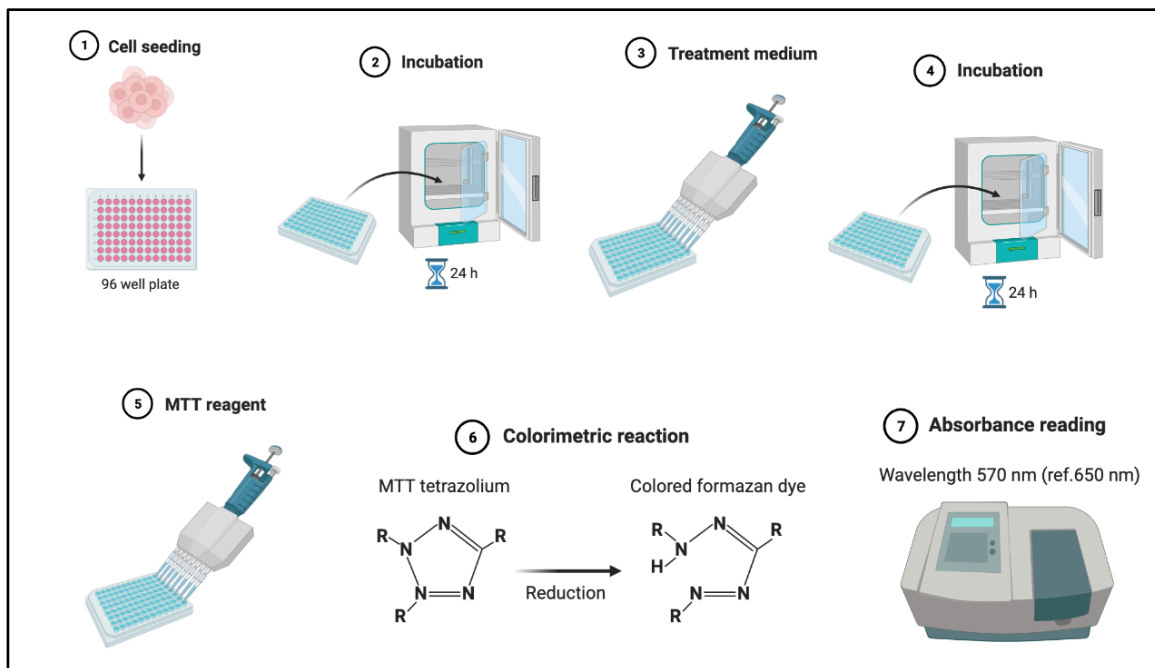


**Figure 5 MTT cell toxicity assay procedure.** The procedure starts with cell seeding on a 96-well plate (1) and subsequent incubation of the plate for 24 hours (2). After the incubation time the treatment media is applied (3). The treated cells are incubated for another 24 hours (4). Afterwards the treatment media is discarded and MTT reagent is applied (5). MTT reagent is then reduced to coloured formazan crystals (6). This change in colour can be measured at a wavelength of 570 nm (7). Created with BioRender.com.

The metabolic activity correlates directly with the amount of blue-violet formazan formed, as monitored by the optical density at 570 nm. For the calculation of viabilities Equation 1 was used.

Equation 1 Viability in percent for cytotoxicity MTT assay

$$\text{Viability \%} = \frac{100 \cdot OD_{570} \text{ of the } x \% \text{ extract}}{OD_{570} \text{ of the blank}} \quad 0 < x < 100 \%$$

If the viability of the 100 % treatment medium group was reduced to less than 70 % of the untreated group, the material was considered cytotoxic. If the viability of the 50 % treatment medium group was calculated less than the viability of the 100 % treatment medium group, the test was repeated.

## 2.4 Nanoparticle tracking analysis

Nanoparticle tracking analysis (NTA) of the PLA printing material was performed to investigate, if the sterilization process of the inserts results in the release of nanoparticles, which can interfere with generation and evaluation of full thickness equivalents.

First, PLA transparent discs with a diameter of 5 mm and a height of 1 mm were printed. These discs were either sterilized in 70 % ethanol for 30 min, sterilized in 70 % ethanol for at least 15 min and additionally irradiated for 30 min under UV light or not treated at all (non-sterile) to compare sterilization techniques. The discs were then incubated each in 2 ml of filtered PBS (fPBS) for 48 h. To filter PBS a 0.22 µm filter system (Corning, USA) was used. A particle tracking analyser, called Zeta View® Quatt (Particle Metrix, Germany) with ZetaView software (Particle Metrix, Germany) was utilized. To start the analyser, the chamber of the NTA was washed once with double distilled water (Fresenius, Austria) and the temperature was set to 25 °C. Then, a daily performance check was done by the injection of 3 ml of a solution containing 110 nm solid polymer microspheres (Microtrac Retsch GmbH, Germany), which were diluted 1:250.000 in double distilled water. Afterwards, the chamber was cleaned with fPBS. The samples were then measured in the NTA device at 488 nm in scatter-mode.

## 2.5 Generation of skin equivalents

Full thickness equivalents were seeded either on in-house 3D printed or on purchased inserts (Falcon® Permeable Support for 6-well plate in BD Falcon™ Deep-well plates (BD Bioscience, USA)), as a control.

To generate a mixed collagen/fibrin loaded with fibroblasts, the fibroblasts were detached according to standard cell culture protocol. The pellet was then resuspended in FCS and a cell suspension with an end concentration of  $5 \cdot 10^5$  cells/ml in the collagen/fibrin gel was prepared. The mixing of the gel was conducted under cold conditions, on ice, to prevent early clotting of the mixture. First, Hank's Balanced Salt Solution (HBSS) with phenol red (Gibco, USA) was added dropwise to collagen (Collagen G, type 1, solution 4 mg/ml (Sigma-Aldrich, USA)). The pH was slowly adjusted with 1 M sodium hydroxide solution until the mixture turned red/pink. The fibroblast/FCS solution was added to the pH adjusted mixture. For the preparation of the collagen/fibrin gel loaded with fibroblasts mixing proportions of one part HBSS, one part fibroblast/FCS suspension and eight parts collagen

were used. To add fibrin, TISSEEL Lyo (Baxter, USA) was used. The thrombin component of the kit was added to fibroblast/FCS suspension to an end concentration of 1 U/ml before adding the mixture to the collagen. To start the gelling, the fibrinogen component of the kit was dissolved in aprotin, according to manufacturer's instruction and added to the final mixture at a concentration of 3 mg/ml. 2 500  $\mu$ l (6-well-plate size) and 400  $\mu$ l (12-well-plate size) of collagen/fibrin gel containing fibroblasts were quickly filled without air bubbles into each insert. Plates, sealed with parafilm were incubated for two hours at 37 °C without CO<sub>2</sub> until the collagen/fibrin matrix was solid. To equilibrate the gel, 2 000  $\mu$ l (6-well-plate size) or 300  $\mu$ l (12-well-plate size) keratinocyte growth medium was pipetted into each insert and the outer well was filled above the membrane level. Equilibration for at least one hour was conducted in the incubator at 37 °C with 5 % CO<sub>2</sub>. Next, for the epidermal layer, keratinocytes were detached according to standard cell culture procedure. A cell suspension of  $1.5 \cdot 10^6$  cells/ml was prepared in keratinocyte culture medium. After the removal of equilibration medium from the inner insert, 1 000  $\mu$ l (6-well plate size) and 300  $\mu$ l (12-well plate size) of keratinocyte suspension was added on top of the solid gel. The SE were then incubated overnight at 37 °C, 5 % CO<sub>2</sub> and moderate humidity. The next day (Day 2), the SE were loosened by moving a 200  $\mu$ l pipette tip carefully around the outer wall of the insert to avoid tension stress during the culturing. On Day 4, the medium was changed from keratinocyte growth medium to differentiation medium. For that, 500 ml KGM medium (Lonza, Swiss) was supplemented with 25 mg ascorbic acid (Sigma-Aldrich, USA), 500 mg Albumin from bovine serum (BSA) (Sigma-Aldrich, USA), 5 mg Transferrin (Sigma-Aldrich, USA) and CaCl<sub>2</sub> (Sigma-Aldrich, USA) to an end concentration of 1.3 mM. The dry components were added to the KGM medium, and the mixture was subsequently filtrated through a 0.22  $\mu$ m filter. Next, the KGM SingleQuot supplements (Lonza, Swiss), except for the Bovine Pituitary Extract (BPE) were added. The differentiation medium was then added only to the outer wells to facilitate the ALI. For this, a volume of 10 ml for commercial plates, 4 ml for the 3D printed 6-well plate size inserts and approximately 500  $\mu$ l for 3D printed 12-well plate size inserts were used. The medium was changed every other day for one to three weeks, depending on the conducted experiments.

## 2.6 Histology

SE together with the insert membranes were transferred to a histology cassette and fixed in formaldehyde 4 % aqueous solution (VWR International, USA) for 24 h. On the next day, the samples were rinsed in tap water for 1 h, followed by dehydration in 50 % ethanol for

another hour. The fixation was completed by storing the biopsy samples in 70 % ethanol. The hematoxylin and eosin (HE) staining and the embedment in paraffin was performed at the University Clinic of Dentistry of the Medical University of Vienna.

## **2.7 Permeability assay**

To perform the permeability assay, the SE in its insert was rinsed twice with PBS. Next, the insert was transferred into a new well plate. A 3D printed permeability ring, described in chapter 3.3 to unify the investigated area of the SE, was clicked into the insert and placed tightly on top of the SE on the membrane. The well was filled with 4.5 ml PBS as a recipient solution to later collect the fluorescent dyes that were able to penetrate the SE. 20  $\mu$ l of dye were added on top of the SE. At each timepoint 100  $\mu$ l of the collection suspension were transferred into a black 96-well plate (Greiner Bio-One, Austria). Fluorescence was measured at 584 nm (reference 620 nm) for Alexa Fluor® and 485 nm (reference 520 nm) for riboflavin. The experiment was conducted under dark conditions. All measurements were taken directly after collection of the material. Used dyes: Riboflavin (Sigma-Aldrich, USA) and Alexa Fluor® (InvitroGen, USA).

## **2.8 Statistics**

Data were tested for statistical significance using One-way ANOVA with Tukey's multiple comparisons test by GraphPad Prism 8 (GraphPad Software, USA).

## 3 Results

### 3.1 Construction of inserts

Fixed requirements (Figure 4) at the beginning of the construction phase were a sufficiently large support surface for the membrane, as well as the possibility of a medium exchange through the membrane. More accurate: the accessibility/flushing of nutrients from the medium from the bottom side of the membrane. Another requirement was that there should be enough space for a certain volume of nutrient medium from the epidermal side inside the insert after adding the collagen hydrogel. Moreover, practical way to exchange media is obligatory, as well as the compatibility with common cell culture plastic ware.

A sufficiently large stand area was constructed for a safe stand in the well plates. To ensure the medium flow, seven ports were integrated into a cylinder. At the upper end of the cylinder, there was a support surface on which any membrane can be placed. To be able to use a large variety of membranes, a snap closure was implemented in the construction. A cylinder with the complementing dimensions was designed for the upper part. The lower part and the upper part form a snap closure to fix the inserted membrane. The first constructions were created fitting into 12-well plates. (See Figure 6)

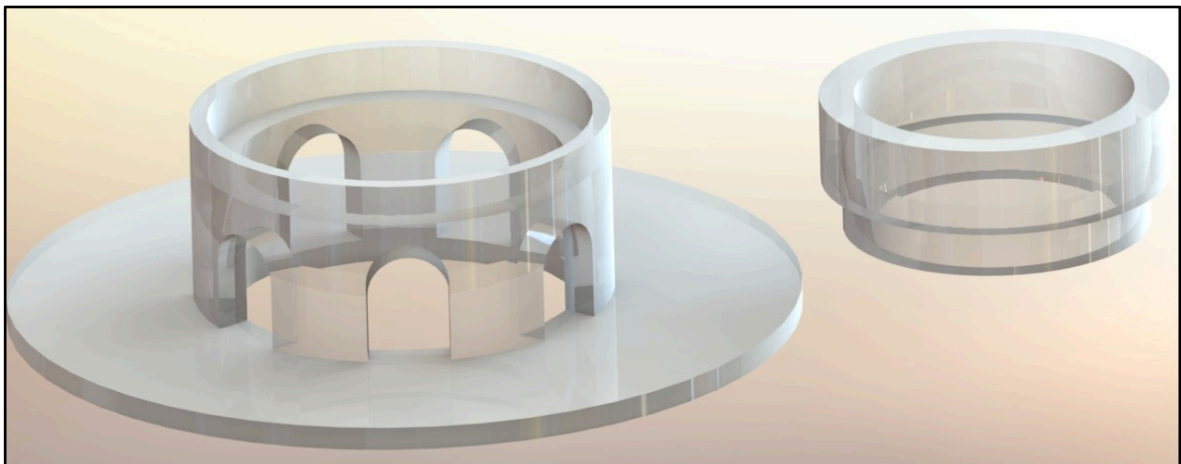


**Figure 6 First construction version of 3D printed inserts.** On the left side the bottom part, with a round stand area and a central cylinder is shown. The cylinder has seven windows and on the upper part, a saving for the cap, which is depicted on the right side. Both fit together perfectly and form a snap closure, in the middle of which any membrane can be clamped. The cells that subsequently form the SE are cultivated on the membrane. Depending on the print size, the insert can be placed in a standard 6-well plate or 12-well plate.

To evaluate the first version, a nucleopore membrane was clamped between the upper and lower part to check the seal. By filling the insert with water, it could be shown that the snap closure sealed well and that the fluid stayed in the inner part of the insert. In these first attempts it could be demonstrated that the space outside the insert required for the medium exchange was not sufficient in this version. The pipette tip of a 10 ml serological pipette was required to fit between the insert and the wall of the well plates. It was also noted that a large number of windows is associated with a higher stringing rate. Stringing is the threading of the print material, outside of the planned print. Based on this knowledge, the next version was adapted.

In this second version, the cylinder with the windows is arranged decentrally on the stand area. To create more space for the pipette tip, the diameter of the cylinder has also been reduced. The number of windows has also been decreased from seven to four. (See second version in [Figure 7](#))

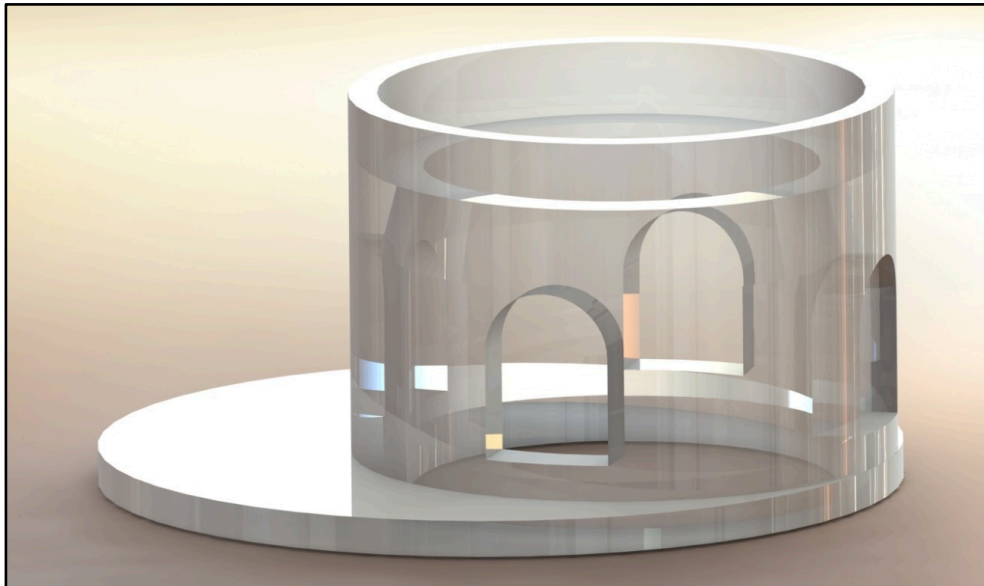


**Figure 7 Second construction version of 3D printed inserts.** This graphic shows an adapted construction version of the bottom section of an insert in 12-well plate size. The cylinder has been decentralized and the number of windows has been reduced from seven to four.

Due to the decentralization of the cylinder, there was now enough space for the pipette tip to exchange the liquid. In the water test it became evident that the four windows also guaranteed a good exchange of fluid. On closer inspection, it became apparent that smaller

air bubbles were accumulating under the membrane. To prevent this, the windows were raised up to the membrane in the following third version.

The windows were enlarged to let out air that could accumulate under the membrane. (See third version in **Figure 8**)

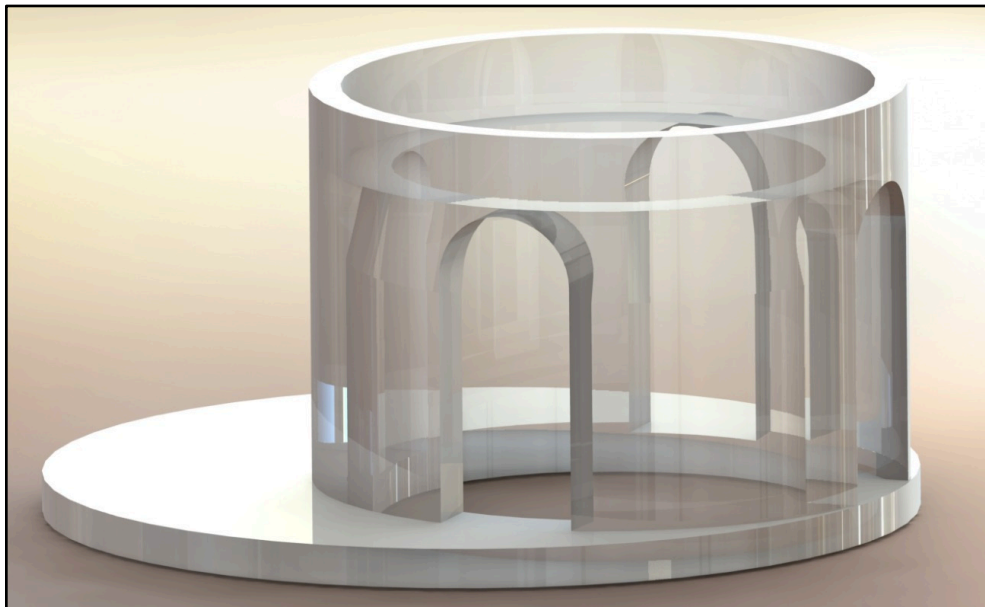


**Figure 8 Third construction version of 3D printed inserts.** Here, an adapted construction version of the bottom section of an insert in 12-well plate size is shown. The windows were enlarged to let out air that could accumulate under the membrane.

The first full thickness SE experiments were started with this third version of the insert, fitting in 12-well plates. See first SE results in chapter 3.5.1.

After the first cell culture attempts, the construction was refined with further small changes. These are shown below, in the larger 6-well plate size of the inserts. To make the practical work easier, a phase has been added to the upper edge of the lower part and the upper part. The resulting groove makes it easier to remove the upper part from the lower part in order to harvest the SE. Furthermore, the cylinder was moved a little more into the middle to make the window, which was located directly on the well plate, accessible. (See fourth version in **Figure 9**)

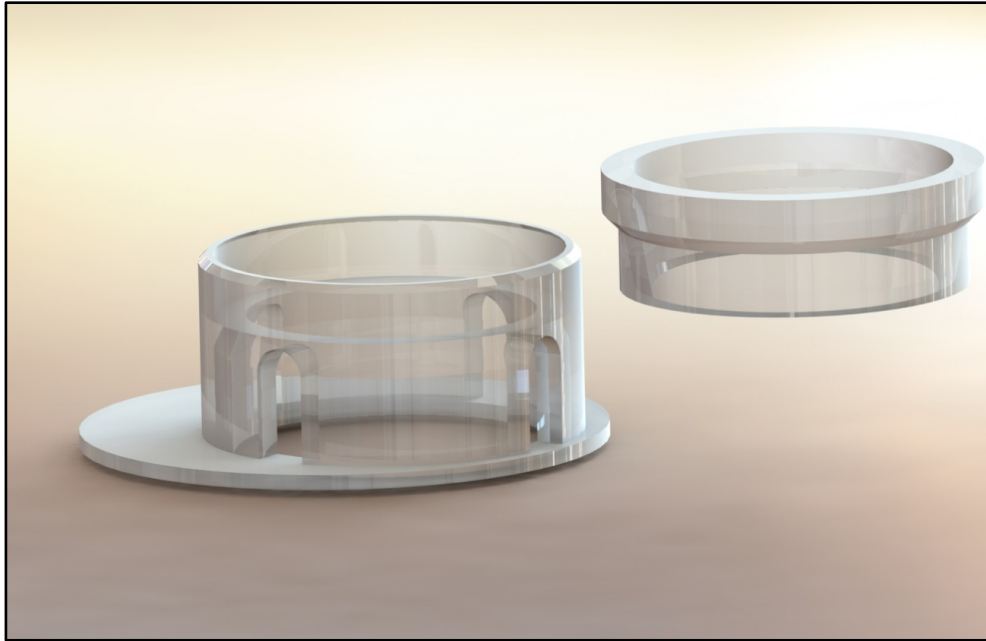


**Figure 9 Fourth construction version of 3D printed inserts.** Here, an adapted construction version of the bottom section of an insert in 12-well plate size is shown. The windows were enlarged to let out air that could accumulate under the membrane. Furthermore, a phase has been added to the upper edge of the lower part and the upper part, creating a groove, which makes it easier to remove the upper part from the lower part in order to harvest the SE. The cylinder was also moved a more into the center of the stand area to make the side window more accessible to the media.

With this version of the insert, cell culture experiments exposed that there was not enough space above the membrane to be filled with collagen/fibroblast gel and subsequent with keratinocyte suspension. In the next construction, the membrane support surface was therefore moved downwards. The contact surface was offset downwards and the surface for the snap closure extended over almost the entire surface of the upper part. (See modified version in **Figure 10**)

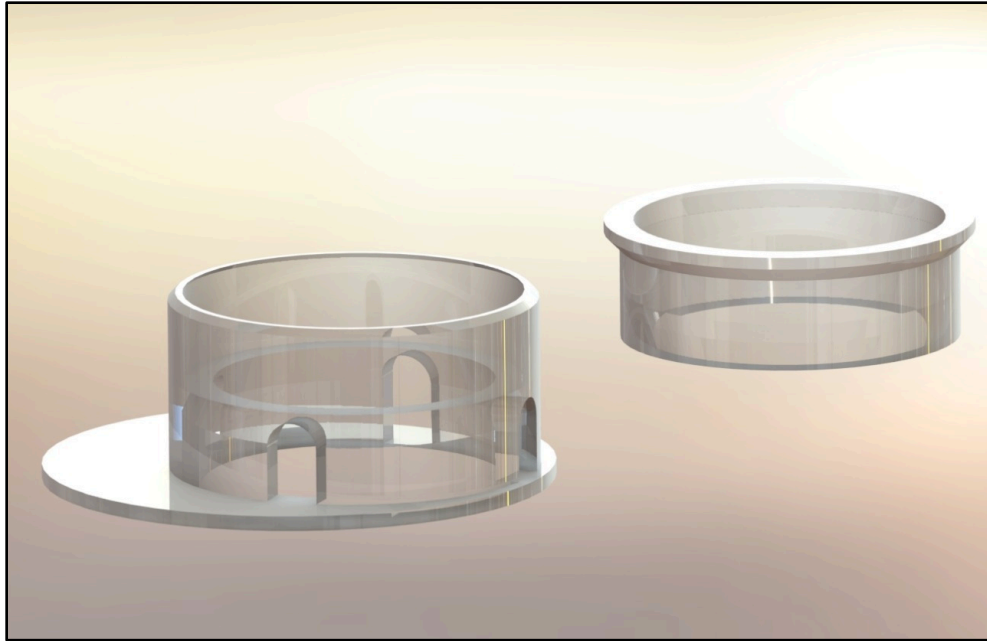


**Figure 10 Fifth construction version of 3D printed inserts.** Both parts of the inserts were improved in this construction step. In order to increase the inner filling volume of the inserts, the membrane support surface was placed further down. Furthermore, the snap closure extends over almost the entire surface of the upper part.

After printing this version for the first time, it quickly became apparent that the large area of the closure caused practical problems. The large clamping surface made it difficult or even impossible to assemble and disassemble the cover.

In the next and final construction, the clamping geometry was changed so that there was less clamping force, thereby making assembly and disassembly easier. Furthermore, the insert volume was expanded a little and the window widened to continue to guarantee a good media flow. (See final version in **Figure 11**)

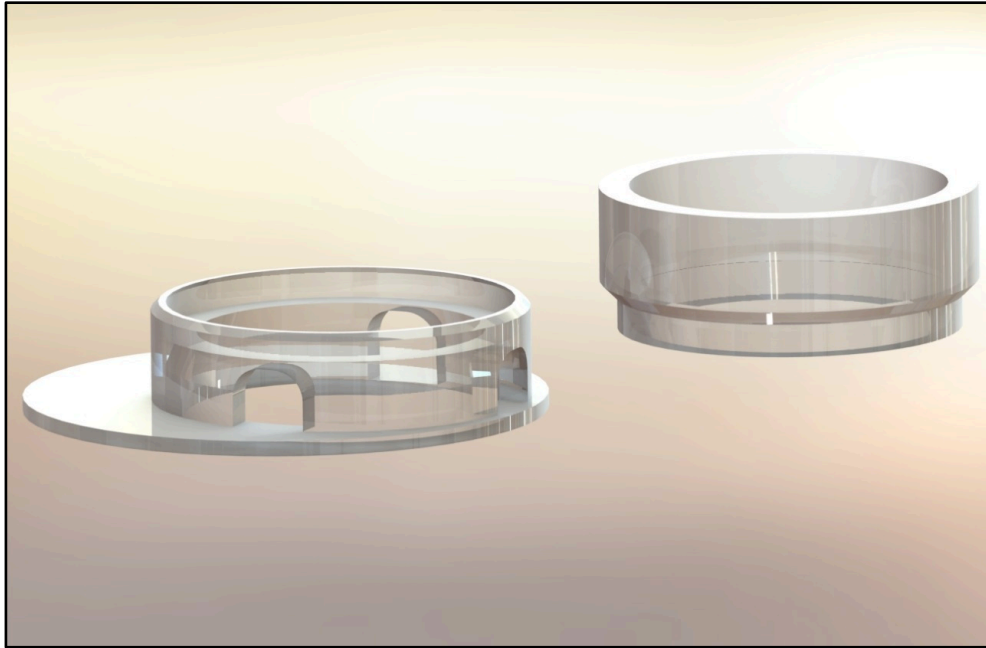


**Figure 11 Final construction version of 3D printed inserts.** Bottom (left) and top (right) part construction of the insert is shown. The bottom part consists out of a round stand area and a decentralized zylinder with four windows. The windows reach the membran area, which is directly on the border of the snap closure. The snap closure connects bottom and upper part. The top part has an increased filling volume compared to the first versions of the construction.

This final construction was used in all experiments (unless stated otherwise). The inside diameter amounts to 1.8 mm, with an area of 2.5 cm<sup>2</sup> it corresponds to the dimensions of the purchased inserts and is therefore directly comparable. The material costs are effectively low.

### 3.2 Excursion twist lock

Not only a snap lock was evaluated for the lock, but also a twist lock. The idea was to improve and simplify the assembly and disassembly of the cover. (See Figure 12)

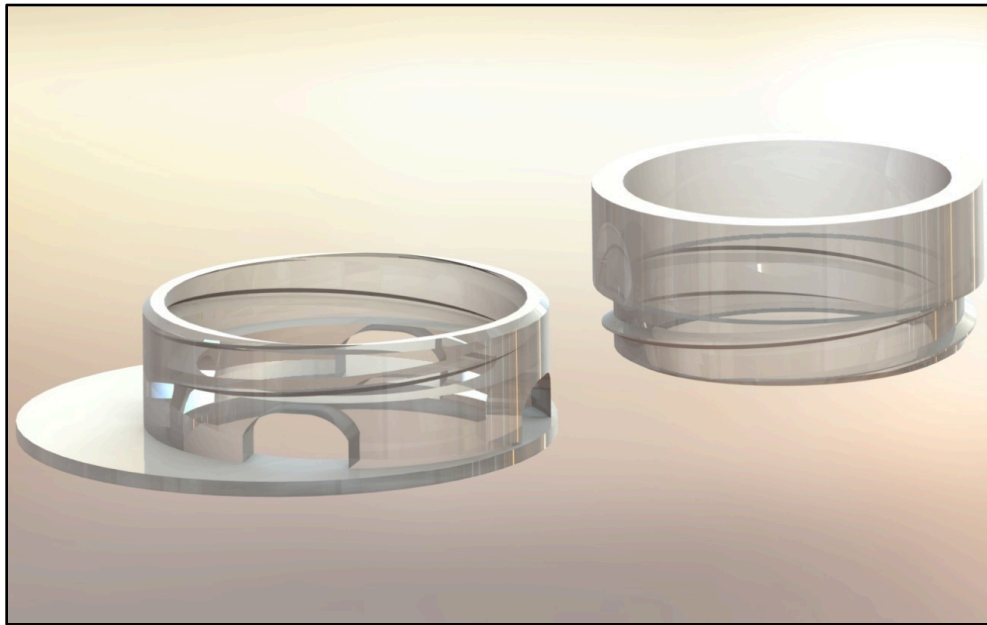


Figure 12 Twist lock construction. Bottom (left) and upper (right) part of a insert with twist lock is shown in this render graphic.

In the first membrane placing attempts it could be seen that the membrane was not stretched properly. In fact, the membrane warps as a result of the rotation and becomes wavy, and sometimes cracked. Based on that, the idea of a screw cap was discarded.

### 3.3 Permeability ring

To test permeability, a test substance is added onto the test material, in this study skin was investigated. The evaluation of the permeability takes place “behind” the material, in a donor cell filled with a reserve solution. The solution is analysed to draw conclusions about the quantity of the test substance. The higher the permeability is, the higher is the content of test substance in the receiver solution.

In order to construct such a permeability assay setup, a PLA ring was constructed. First tests revealed that only the insert was not eligible for this application. The ring was necessary, due to the shrinking of the full thickness SE. The test substance would not pass the SE but choose the free membrane space on the borders of the SE after SE shrinking to pass into the

receiver solution. This ring should unify the test area of the SE and exclude possible edge effects of the SE. The ring should be placed inside the insert and was designed in such a way that the underside rests exactly on the membrane. Thus, the SE was clamped between the membrane and the ring and only a defined area is exposed to a test compound. Moreover, the clamping is intended to prevent potential test substances from running past the side. This is to ensure that the test substances must cross the skin barrier to arrive in the well.

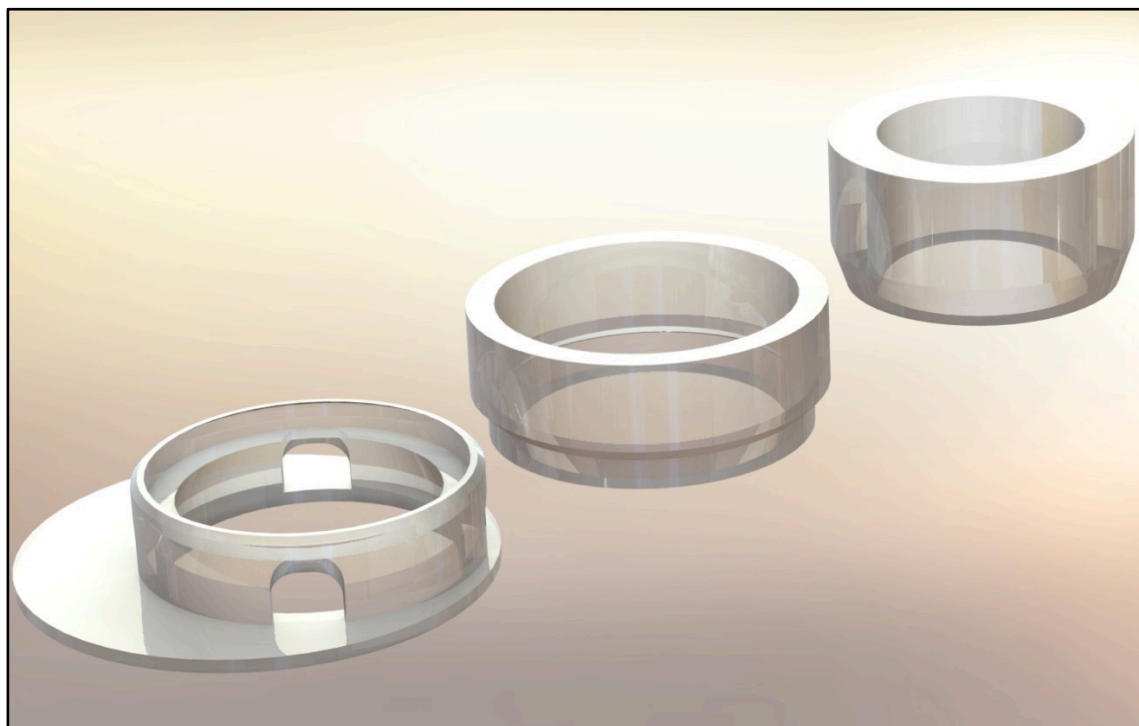


**Figure 13** Final construction of 3D printed inserts together with the permeability ring. From left to right: construction of the bottom section of the insert, which can be connected via a snap closure to the top part of the insert. After the generation of SE on the insert membrane, the permeability ring can be pushed into the top part of the insert. This clamps the SE, excludes edge effects, and standardizes the assay through a defined area.

In **Figure 13**, the final construction of the insert system together with the permeability ring is depicted. The idea was to implement an assay in which the SE does not have to be transferred to a new setup as this can distort the SE. Additionally, an important aspect was the prevention of leakage of test substances at the side. Nevertheless, it is also possible to clamp other materials, such as biopsied skin, into the system. Results of the permeability assay setup are described in chapter 3.5.4.

## **3.4 Evaluation of printing material**

### **3.4.1 Evaluation of cytotoxicity**

No cytotoxic effects of PLA transparent material on keratinocytes or fibroblast in their respective media could be identified according to ISO standard number 10993-5. Furthermore, previously used material did not show any signs of cytotoxic effects.

### **3.4.2 Nanoparticle tracking analysis**

To investigate the potential release of nanoparticles by the PLA transparent filament, NTA analysis was performed in fPBS after an incubation time of 24 h (**Figure 14**). As control, fPBS was analysed with a mean concentration of  $116\,667 \pm 247\,487$  particles/ml. Additionally, two sterilization procedures were investigated (1) PLA pellets rinsed with ethanol (EtOH), resulting in a mean concentration of  $129\,630 \pm 197\,708$  particles/ml and (2) PLA pellets rinsed with EtOH and subsequently UV irradiated, leading to a mean concentration of  $448\,148 \pm 351\,503$  particles/ml. Pellets without sterilization treatment revealed a mean concentration of  $931\,481 \pm 758\,813$  particles/ml. This value differs significantly (with  $P \leq 0.01$  for EtOH sterilized and PBS only group,  $P \leq 0.001$  for EtOH and UV sterilized group) from all other investigated groups. However, washed and UV treated inserts did not result in significantly higher particle release compared to fPBS alone. These results would suggest that the sterilization process used in this work did not trigger the release of particles that could interfere with the generation and histological evaluation of full thickness SE.

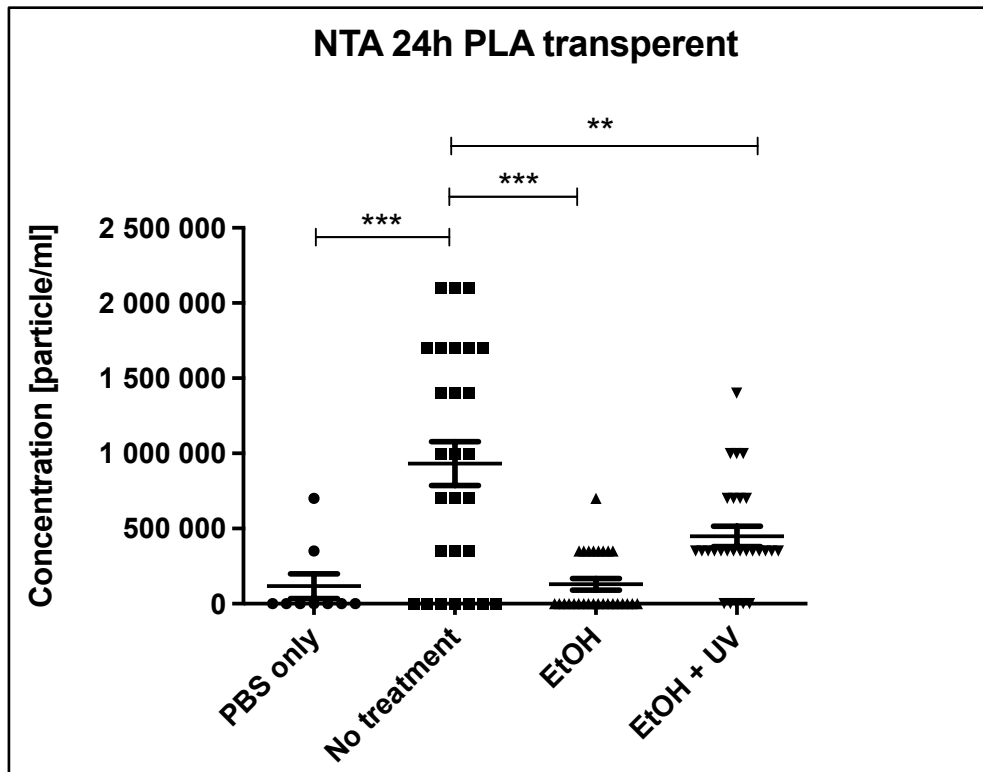


Figure 14 Nanoparticle tracking analysis (NTA) of polylactic acid (PLA) printing filament after an incubation period of 24 hours. PLA pellets were incubated at 37 °C after either no sterilization treatment, rinsing with ethanol (EtOH) or rinsing with EtOH and subsequent UV irradiation. These were compared to filtered PBS (fPBS) without any exposure to PLA. Treated groups did not exhibit signs of nanoparticle release compared to fPBS. Pellets without sterilization treatment released a significant concentration [particle/ml] of nanoparticles compared to all other groups. n = 9 in PBS group n = 27 in treatment groups, \*\* P ≤ 0.01, \*\*\* P ≤ 0.001

### 3.5 Generation of full thickness skin equivalents

#### 3.5.1 Pilot trails of 3D printed vs. commercial inserts

After successful construction of inserts and cytotoxicity testing, we next aimed to generate functional full thickness SE on the in-house 3D printed inserts in cell culture. For the first pilot tests, the third version of the construction was used (see construction in chapter 2.1). In Figure 15 the results of the full thickness SE after HE staining are shown.



**Figure 15 Hematoxylin and eosin (HE) staining of pilot experiments on full thickness skin equivalents (SE) generated in 3D printed.** The epidermis (purple) on top of the collagen matrix harboring few fibroblasts (light pink). The membrane material (transparent) was not removed for the histological analysis. Cultured on a 3D printed 12-well plate insert is depicted. Harvested on ALI day 10, seeded with a concentration of  $3 \cdot 10^4$  fibroblasts/ml in a collagen matrix on a polycarbonate membrane. SE showed the formation of an epidermis and dermis, albeit lacking the defined stratified layers of differentiated keratinocytes. In both cases only a few fibroblasts can be seen in the dermis.

For reference, the same protocol was carried out on purchased inserts in parallel and evaluated (**Figure 16**). Due to the different sizes of the inserts, different volumes of collagen gel were used. This resulted in a different layer thickness of the dermis. The number of fibroblasts also differed in this pilot test. The exact seeding parameters were adapted and refined in later experiments (see chapter 3.5.3).

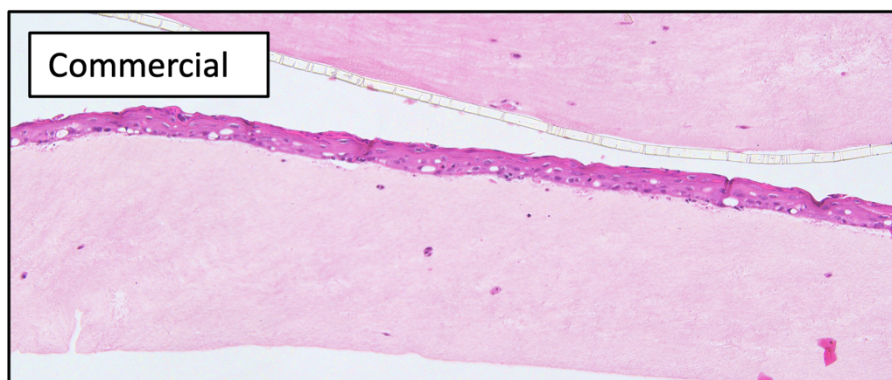


**Figure 16 Hematoxylin and eosin (HE) staining of pilot experiments on full thickness skin equivalents (SE) generated in commercial inserts.** The epidermis (purple) on top of the collagen matrix harboring few fibroblasts (light pink). The membrane material (transparent) was not removed for the histological analysis. SE, generated on a 6-well plate bought insert. Seeding number of  $1 \cdot 10^5$  fibroblasts/ml in a collagen matrix on a polyethyleneterephthalat (PET) membrane. SE showed the formation of an epidermis and dermis, albeit lacking the defined stratified layers of differentiated keratinocytes. Like in SE, cultured on a 3D printed insert only a few fibroblasts can be seen in the dermis.

This first experiment showed the feasibility 3D printed inserts with a polycarbonate membrane. The formation of an epidermis by keratinocytes was observed on the collagen matrix. There were also beginnings of the formation of a *stratum corneum*, as elongated keratinocytes could be detected on the upper side of the SE (Figure 15 and Figure 16). However, there were no distinct layers of other keratinocyte differentiation stages. Very few fibroblasts were found in the dermis. The refinement and further development of the production of full thickness SE are described in the following chapters.

### **3.5.2 Media condition testing**

To investigate the impact of media on the number of fibroblasts, the viability and morphology of fibroblasts was tested in different media. Since fibroblasts are exposed to keratinocyte medium during the cultivation of SE, the main interest in this experiment was to investigate if and how long fibroblasts survive in keratinocyte medium. The media condition tests were carried out in monolayer cultures of fibroblast and keratinocytes. The tested media were (1) keratinocyte and (2) fibroblast specific growth medium, as well as (3) a 1:1 mix of both media. Cells were incubated for 5 days at 37 °C, 5 % CO<sub>2</sub>. The analysis of the results was first conducted visually, assessing cell confluency (Figure 17) in four biological replicates, including each two technical replicates.

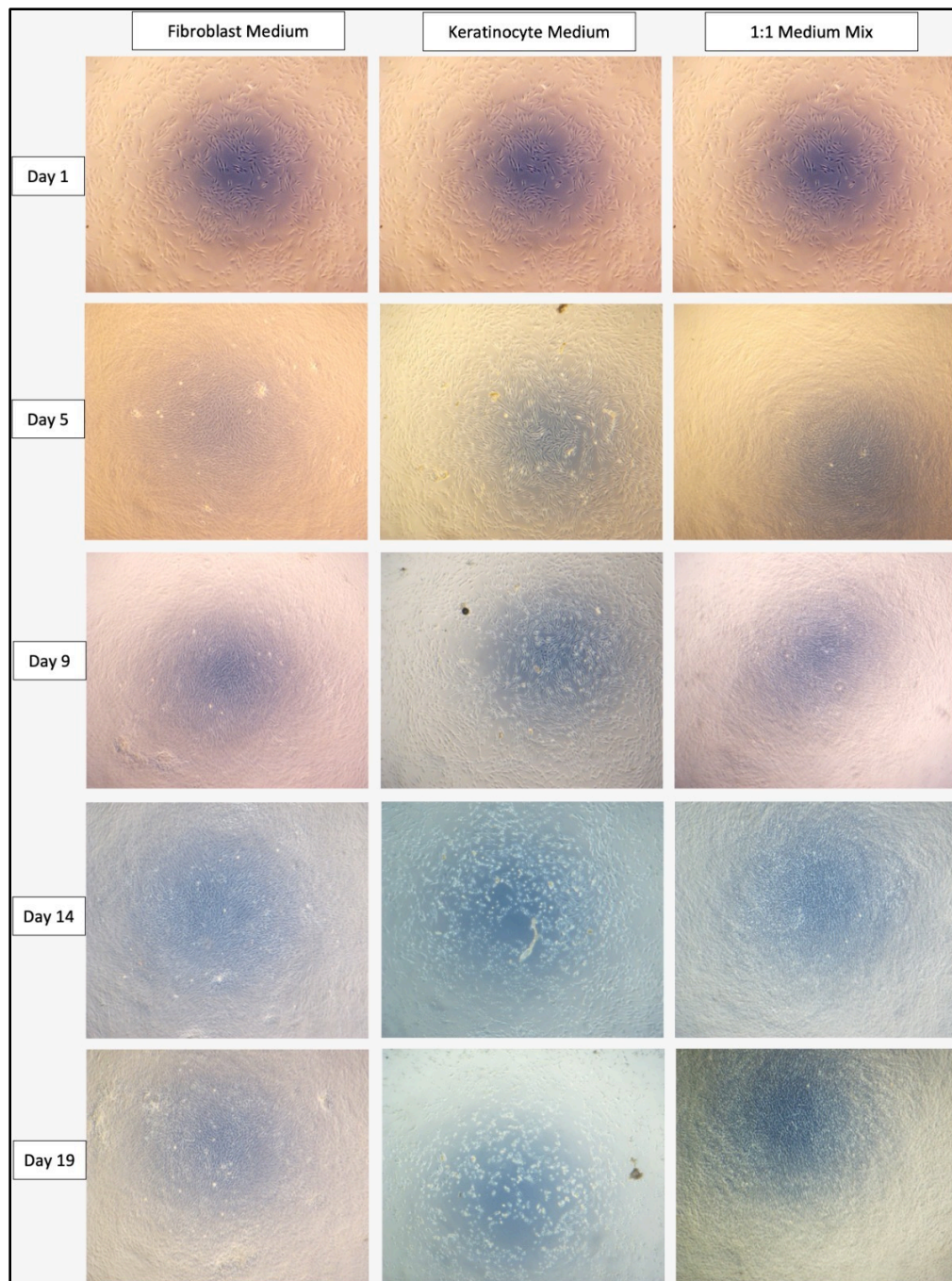


**Figure 17 Visual assessment of cell confluency, as well as morphology of fibroblast monolayers cultured under different media conditions.** Investigation of monolayers cultured in keratinocyte and fibroblast specific growth media, as well as a 1:1 mix of both media for a period of 19 days at 37 °C, 5 % CO<sub>2</sub> and moderate humidity. Pictures were taken on days 1, 5, 9, 14, and 19. Fibroblasts exhibited less proliferation in keratinocyte specific growth media. n=8

The investigation under the light microscope indicated that fibroblasts divided less in keratinocyte growth medium in contrast to the usual culture conditions. Surprisingly,

fibroblasts showed a higher growth rate in a 1:1 mix of fibroblast and keratinocyte growth medium. Keratinocytes divided the most under physiological culture conditions in keratinocyte media and less in fibroblast and 1:1 mixed medium. These findings are supported by the data of an MTT assay with two technical replicates (See Figure 18).

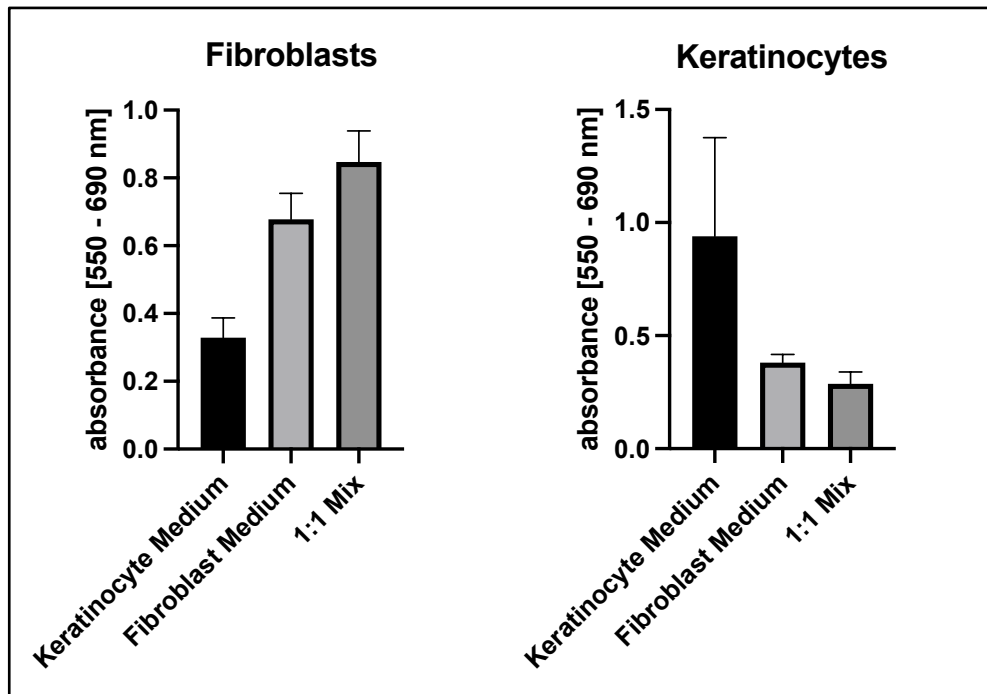
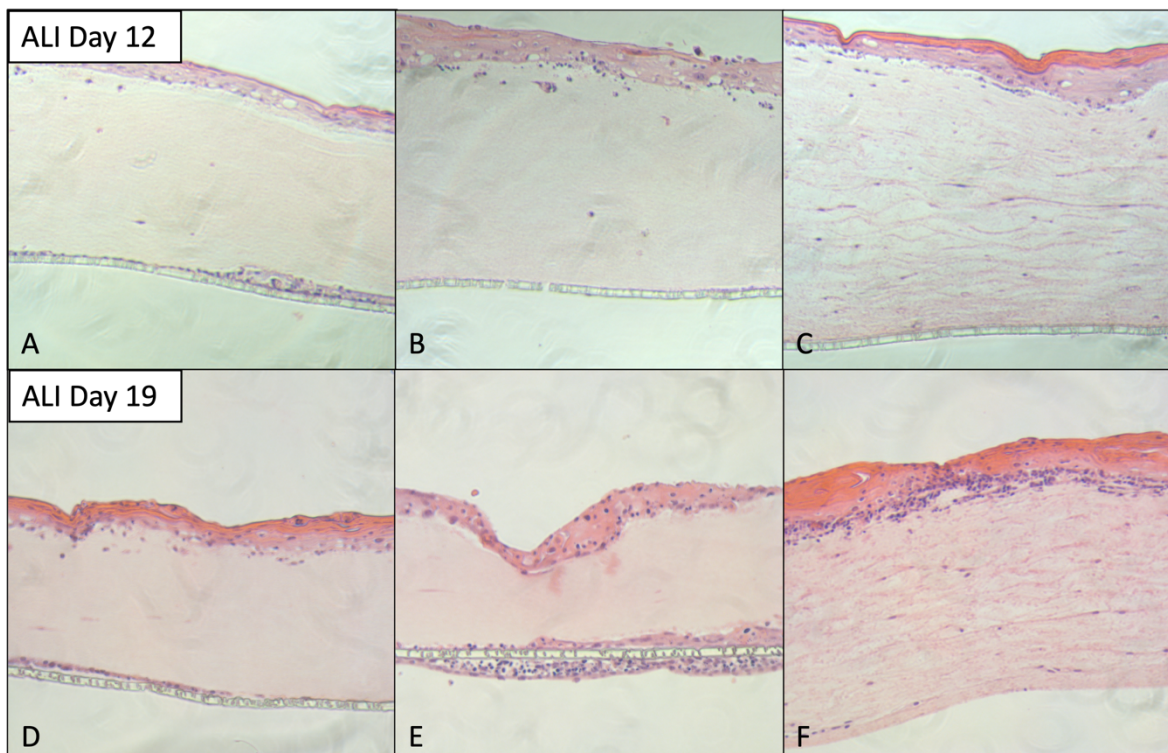


Figure 18 Thiazolyl blue tetrazolium bromide (MTT) assay of fibroblast and keratinocytes monolayers cultured under different media conditions. Investigation of monolayers cultured in keratinocyte and fibroblast specific growth media, as well as a 1:1 mix of both media for 5 days at 37 °C, 5 % CO<sub>2</sub> and moderate humidity. Fibroblasts exhibited less viability in keratinocyte specific growth media. In contrast keratinocytes had the highest viability under these conditions. n=2

### 3.5.3 Refinement of skin equivalent generation procedure

After it could be shown that it was possible to successfully grow SE on the 3D printed inserts, the aim was to refine the procedure, by varying the tested parameters (i.e., type of matrix for the dermis, the fibroblast concentration, and the time intervals between the work steps). Figure 19 shows, full thickness SEs produced with an initial fibroblast concentration of  $1 \cdot 10^5$  fibroblasts/ml or  $5 \cdot 10^5$  fibroblasts/ml. Furthermore, two different timepoints of harvesting the SE were compared. They were harvested on either day 12 or day 19 on ALI. In one group, the fibroblasts were seeded within a fibrin-collagen gel. It turned out that higher seeding numbers of fibroblasts did not result in a visibly denser population of cells in

the hydrogel. This lack of fibroblasts was already seen in the pilot tests. There was evidence that the fibroblasts were seeping down the gel (Figure 19). The histological slides showed an accumulating of cells on the membrane at the bottom of the hydrogel (Figure 19 A, B, D, E). In contrast to this, in the group (Figure 19 C, F) with the added fibrin, it can be seen that the fibroblasts were more distributed in the dermis. Fibroblasts are scattered in the matrix, visualized as purple-coloured cells. Furthermore, the stratum corneum was more distinct in groups, that were harvested on day 19 on the ALI, especially on top of the fibrin-collagen dermis.



**Figure 19** Hematoxylin and eosin (HE) staining of full thickness skin equivalents (SE) on day 14 compared to day 19 on air liquid interface (ALI) testing different seeding parameters. All SE were cultured on commercial 6-well plate size insert and the keratinocytes, forming the epidermis, were seeded immediately after hydrogel polymerization. A & D: fibroblast seeding concentration of  $1 \cdot 10^5$  fibroblasts/ml in a collagen matrix. B & E: fibroblast seeding concentration of  $5 \cdot 10^5$  fibroblasts/ml in a collagen matrix. C & F: fibroblast seeding concentration of  $1 \cdot 10^5$  fibroblasts/ml in a fibrin-collagen matrix. Epidermis (purple) on top of a fibroblasts (fibrin-) collagen matrix (light pink) on membrane material (transparent bottom layer).

In addition, a group in which the keratinocytes were applied one week after seeding the dermis (data not shown), was examined. However, in this experiment the keratinocytes did

not form an epidermis. The keratinocyte suspension seemed to have flown past the edge of the SE. As a result, the cells could not adhere to the surface of the gel matrix and differentiate.

In conclusion, the parameters with the best outcome could be evaluated. The best results were achieved with a (1) initial fibroblast concentration of  $5 \cdot 10^5$  fibroblasts/ml, (2) a dermis matrix made of collagen with fibrin, and (3) a harvesting time point on day 19 or later.

#### **3.5.4 Establishment of skin barrier assay**

To test the functionality and handling of the permeability ring, two groups of full thickness SE in 6-well plates, seeded with  $5 \cdot 10^5$  fibroblasts/ml in a 3.2 mg/ml collagen + 3 mg/ml fibrin matrix, harvested on day 22 of ALI, and different fluorescent dyes were used. On one hand an intact skin barrier was modelled by the investigation of a full thickness SE, treated with Alexa Flour<sup>®</sup> dissolved in water. On the other hand, an irritated barrier was simulated with riboflavin dissolved in DMSO. DMSO weakens the barrier over time and makes it more permeable.

This setup was chosen to simulate both scenarios, intact and dysfunctional barrier, and to test the compatibility with the permeability ring. **Figure 20** shows the fluorescence readout at different timepoints compared to PBS, which was used as a recipient solution in the well plate below the SE to collect the dyes. Furthermore, the absorbance of the starting/maximal concentration, which was applied to the SE, is depicted. It shows that the model of the intact skin did not leak any dye, as the absorbance was in the range of PBS over a period of two hours. The SE treated with DMSO showed an almost linear increase of fluorescence of riboflavin collected after penetrating the SE.

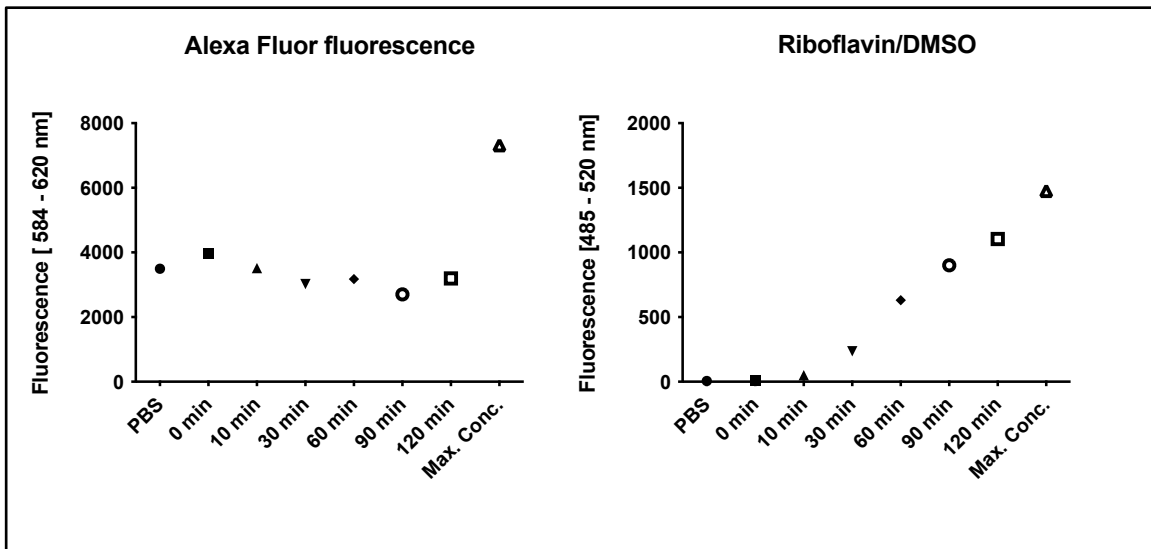


Figure 20 Pilot tests of skin barrier assay with a 3D printed permeability ring using fluorescent measurements of Alexa Fluor<sup>®</sup> and Riboflavin/DMSO. Left: Intact skin barrier was provided with Alexa Fluor<sup>®</sup>. Right: Skin barrier was irritated with DMSO, and permeability was tested with riboflavin. In contrast to the intact SE, an almost linear increase in fluorescence can be seen. Measurements were taken at different timepoints from zero minutes to two hours. Furthermore, PBS as well as the highest possible concentration of fluorophores (Alexa Fluor<sup>®</sup>: 10 mg/ml, riboflavin: 1 mM) was measured. Fluorescence was measured at 584 nm (reference 620 nm) for Alexa Fluor<sup>®</sup> and 485 nm (reference 520 nm) for riboflavin.

These experiments indicate that the 3D printed ring is suitable for a permeability assay of irritated and intact skin.

## 4 Discussion

Just now there is a great demand to close the *in vitro*–*in vivo* gap in the biomedical research landscape. Therefore, novel *in vitro* model systems that can be used to accurately represent and forecast physiological behaviour of healthy and diseased skin tissue move into the focus of research. In the spirit of the 3R's new approaches are inevitable. The present study contributes a puzzle piece to the generation of in-house full thickness SE using the clinically relevant method of 3D printing, as well as testing of functional the skin barrier.

Few examples of the utilization of 3D printing technologies to solve cell culture related tasks can be found in current literature. Grottkau et al. utilized stereolithography 3D-printing technology to manufacture a 3D printed insert-array and a 3D coculture-array for high-throughput screening of cell migration [40]. Li et al. established a microscale scaffold for cell culture with E-Jet 3D printing technique [41]. In the present study we could successfully demonstrate that our manufacture method – extrusion-based FDM 3D printing of transparent PLA – is suitable to generate cell culture inserts. This technique was chosen due to its specific benefits such as operational simplicity, customizable design, operational safety, cost-effectiveness and diversity of the compatible materials [42]. Extrusion-based printing has a relatively low resolution compared to most other 3D printing methods, like photopolymerization techniques (PPT). PPT are the most commonly used processes in dental applications, providing high resolution, allowing very fine surface finish and the ability to create complex shapes [43]. However, these parameters do not leave such high priority like in dental medicine. The benefit from operational simplicity, and operational safety outweighs by far.

First, a computer-aided design model was created. While improving the insert, we went through six construction versions. Modifications after the testing of each version improved the insert from a pilot device all the way to the final operative version.

For all cell culture materials, the choice of the used material is important. PLA is used more and more for medical applications, like wound management [44], stent applications [45], as well as orthopedic and fixation devices [46], tissue engineering [47] and drug delivery [48], but also finds wide use in the non-medical field [44]. PLA takes ten months to four years to degrade in the human body, depending on the microstructural factors, like chemical

compositions porosity and crystallinity [49]. This agrees with our observations that the inserts remain stable over the cultivation period. The PLA degradation products, mainly lactic acid is known to be non-toxic (at lower composition). We know from many previous studies and the chemical structure that the material is inert due to its lack of reactive side-chain groups [50]. This makes the material a natural choice for biomedical applications. We confirmed this knowledge with cytotoxicity test according to ISO 10993-5, where no cytotoxic effects could be seen given our experimental conditions. Moreover, the material did not release nanoparticle, tracked with NTA, during sterilization procedure. The data area consistent with Mizielińska et al., who could not see changes in the mechanical properties of PLA after UV-A and Q-UV irradiation [51]. Nanoparticle could interfere during the seeding procedure or the histological analysis. Grant et al. investigated skin tissue and fibroblasts for tattoo ink nanoparticles. Nanoparticle are visible in histology sliced skin [52] and could probably interfere with analysis. In the present study, we confirmed with NTA no nanoparticle release of PLA material. Concluding, that light microscopy analysis is free from interference of material nanoparticle.

In the human body, cells are surrounded by the extracellular matrix (ECM). This ECM must be simulated in 3D tissue engineering. Collagen is the major structural protein of most hard and soft tissues in the human body. It plays a prominent role in maintaining the structural integrity, as well as the biological function of the ECM [53]. Moreover, collagen provides physical support to tissues and with around 30% of all proteins it is the most abundant protein in mammalian bodies [54]. In the beginning collagen type I was used to model the ECM of the dermis. Fibroblasts were seeded into the collagen gel. The histology results revealed that the fibroblast disappeared within the incubation time of the SE. Media condition test showed, that this could be due to the use of keratinocyte medium. In 2D monolayer cultures fibroblast cultured with keratinocyte medium revealed morphological changes and lower numbers of proliferation (**Figure 17**). Another explanation for the low number of fibroblasts that outlasts the long incubation times of up to three or four weeks, lays in the EMC. There is evidence, that cells sunk down in the collagen and assembled at the membrane (**Figure 19**). In contrast, fibroblasts were more distributed in higher cell numbers within in the dermis, consisting out of collagen-fibrin gel. Fibrin and Fibrinogen play a role in haemostasis and are main factors of wound healing, and several other biological functions, like thrombosis [55]. Fibrinogen

is a large glycoprotein, which is cleaved by thrombin converting the soluble molecule to insoluble fibrin [56]. As fibrinogen has been shown to contain RGD integrin binding sites which commonly bind fibroblasts [57], the acceleration and enhanced viability is explicable.

With the first cell culture experiment it was successfully demonstrated that it is technically possible to generate SE on the in-house 3D printed inserts. The formation of an epidermis created by keratinocytes could clearly be detected on the collagen matrix. There were also beginnings of the formation of a *stratum corneum*. This could be seen in elongated keratinocytes on the upper side of the SE. To further test the functionality of the in-house generated full thickness SE the skin barrier was examined, performing skin permeability assays.

The skin barrier is one of the major functions of the skin. To investigate the nature of the barrier *ex vivo*, immunohistochemistry and immunofluorescence stainings [58], as well as HE staining [59] can be performed. A non-invasive method is a test for transdermal electrical resistance [60]. Moreover, RNA expression of skin barrier related proteins, amongst many others filaggrin-, filaggrin-2 and loricrin [61] can be examined via qRT-PCR. Filaggrins are structural proteins of *stratum corneum*, which plays a key role as top layer of the skin in barrier function [62]. Loricrin is a terminally differentiating structural protein that can be found in the cornified cell envelope and it is expressed in all mammalian stratified epithelia [61, 62]. Currently the golden standard to investigate permeability of skin barrier and transdermal drug administration quantitatively is a Franz diffusion cell (See **Figure 21**) [65]. After clamping membrane and/or the sample into the apparatus the testing substance is applied in the donor compartment. Sample collection is conducted through a sampling port from the receptor compartment, containing a magnetic stirrer [66]. There are also approaches in which such a cell can be successfully 3D printed. Sil et al. successfully printed a diffusion cell in a proof-of-concept study using stereolithography technique [67].

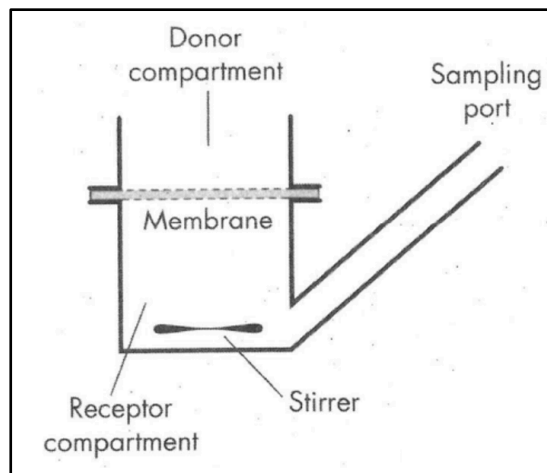


**Figure 21 Franz diffusion cell.** Perfusion material or dye is applied to the donor compartment and detected in the receptor compartment after passing the membrane or sample material. The receiver solution is mixed with a stirrer. Samples selection takes place via a sampling port. Taken from [66]

We aimed to modify the in-house insert system to be used as a Franz cell-like system to investigate the functionality of the full thickness SE. Therefore, a permeability ring was constructed and printed, to unify the test area of the SE and exclude possible edge effects of the SE. The first experiments confirmed that the ring seals the test system and is suitable to test healthy and diseased skin models. Compared to the established Franz cell the advantage of the described in-house system, is that the skin barrier assay can be conducted without the laborious transfer of the SE onto a new system. Nevertheless, it is also possible to clamp in other samples or materials into the in-house system.

In the present study we aimed to create a method, that provides the possibility to model impaired and healthy skin barrier. To test diseased skin, the well-known penetration enhancer DMSO was utilized [68]. DMSO can denature skin proteins, thus disturbing the integrity of corneocytes and their desmosomes. Moreover, DMSO is an amphiphilic molecule, interacting strongly with the lipid bilayers, changing its packaging geometry. Long exposure to DMSO can lead to skin irritations and long-term damages of human skin [69]. Due to its solubility in DMSO, riboflavin was used as fluorescent dye. Riboflavin is a known substance to test skin barrier properties. Nakamura et al. performed the stripping method to test barrier function. For the stripping method stratum corneum was stripped with adhesive cellophane tape. To extract the riboflavin from the tape sodium dodecyl sulphate solution and sonication was used. The concentration of riboflavin was determined by measuring the fluorescence of riboflavin in the extract solution [70]. In this study the healthy

skin was modelled with the untreated full thickness skin equivalent and the florescent dye Alexa Fluor<sup>®</sup>, which was also used before to test transdermal drug delivery [71].

The skin barrier consists of complementing components: a physical barrier in particular localised in the epidermis, and an immune barrier in both the dermis and epidermis [72]. A limitation of this study is, that the immune component of the skin barrier was not considered. As an extension, however, it is possible to integrate the immune component into the 3D printed system. There are many examples in the literature in which parts of the immune system are integrated into artificial SE. The simplest method would be to add relevant cytokines but there are also approaches with incorporated Langerhans cells [73], dermal dendritic cells [74], T cells [29], and macrophages [75]. Moreover, the replicate number of experiments, conducted using the permeability ring is limited. The described experiments can only give a definitive statement about the technical function and handling of the 3D printed ring. To integrate the in-house skin barrier system into the daily laboratory life, the system must be evaluated further.

Refinement of the skin barrier assay is planned. A direct comparison to a Franz diffusion cell – the golden standard – can be used. It is unknown, if and to which extent the magnetic stirrer in the receptor compartment changes the outcome of experiments. Franz diffusion cell could be 3D printed as well, described in [67], to evaluate, whether the lack of stirring in the well plate contributes to the outcome of the assay. Moreover, further evaluation of the transparent PLA material is currently conducted to investigate, namely lactic acid release from PLA and its effects on viability of SE.

To conclude: in the present study a novel 3D-printed insert device for advanced skin regeneration cell culture models was successfully established and evaluated. As extension it is possible to add a permeability ring to straightforward test skin barrier function. The system is accessible to everyone with a 3D printer. The in-house 3D printed system is compatible to commonly used cell culture plates and greatly cost-effective. Compared to commercially available inserts, one can choose the preferred printing material, membrane material, as well as the required size and therefore make various scientific questions accessible.

## Bibliography

- [1] L. M. Biga *et al.*, “5.1 Layers of the Skin,” in *Anatomy & Physiology*, OpenStax/Oregon State University, 2019. Accessed: Jun. 15, 2021. [Online]. Available: <https://open.oregonstate.edu/aandp/chapter/5-1-layers-of-the-skin/>
- [2] H. Sorg, D. J. Tilkorn, S. Hager, J. Hauser, and U. Mirastschijski, “Skin Wound Healing: An Update on the Current Knowledge and Concepts,” *Eur Surg Res*, vol. 58, no. 1–2, pp. 81–94, 2017, doi: 10.1159/000454919.
- [3] M. J. Randall, A. Jüngel, M. Rimann, and K. Wuertz-Kozak, “Advances in the Biofabrication of 3D Skin in vitro: Healthy and Pathological Models,” *Front. Bioeng. Biotechnol.*, vol. 6, 2018, doi: 10.3389/fbioe.2018.00154.
- [4] H. Yousef, M. Alhaji, and S. Sharma, “Anatomy, Skin (Integument), Epidermis,” in *StatPearls*, Treasure Island (FL): StatPearls Publishing, 2021. Accessed: Sep. 18, 2021. [Online]. Available: <http://www.ncbi.nlm.nih.gov/books/NBK470464/>
- [5] A. L. Byrd, Y. Belkaid, and J. A. Segre, “The human skin microbiome,” *Nat Rev Microbiol*, vol. 16, no. 3, pp. 143–155, Mar. 2018, doi: 10.1038/nrmicro.2017.157.
- [6] E. S. Chambers and M. Vukmanovic-Stejic, “Skin barrier immunity and ageing,” *Immunology*, vol. 160, no. 2, pp. 116–125, Jun. 2020, doi: 10.1111/imm.13152.
- [7] A. K. Dąbrowska, F. Spano, S. Derler, C. Adlhart, N. D. Spencer, and R. M. Rossi, “The relationship between skin function, barrier properties, and body-dependent factors,” *Skin Res Technol*, vol. 24, no. 2, pp. 165–174, May 2018, doi: 10.1111/srt.12424.
- [8] R. Agrawal and J. A. Woodfolk, “Skin Barrier Defects in Atopic Dermatitis,” *Curr Allergy Asthma Rep*, vol. 14, no. 5, p. 433, May 2014, doi: 10.1007/s11882-014-0433-9.
- [9] H. A. Hadi, A. I. Tarmizi, K. A. Khalid, M. Gajdács, A. Aslam, and S. Jamshed, “The Epidemiology and Global Burden of Atopic Dermatitis: A Narrative Review,” *Life (Basel)*, vol. 11, no. 9, p. 936, Sep. 2021, doi: 10.3390/life11090936.
- [10] M. Augustin *et al.*, “Epidemiology and Comorbidity in Children with Psoriasis and Atopic Eczema,” *DRM*, vol. 231, no. 1, pp. 35–40, 2015, doi: 10.1159/000381913.
- [11] M. A. Radtke, I. Schäfer, G. Glaeske, A. Jacobi, and M. Augustin, “Prevalence and comorbidities in adults with psoriasis compared to atopic eczema,” *J Eur Acad Dermatol Venereol*, vol. 31, no. 1, pp. 151–157, Jan. 2017, doi: 10.1111/jdv.13813.
- [12] W.-H. Boehncke and M. P. Schön, “Psoriasis,” *Lancet*, vol. 386, no. 9997, pp. 983–994, Sep. 2015, doi: 10.1016/S0140-6736(14)61909-7.
- [13] C. Jacob *et al.*, “Epidemiology and Costs of Psoriasis in Germany – A Retrospective Claims Data Analysis,” *Value in Health*, vol. 19, no. 7, p. A566, Nov. 2016, doi: 10.1016/j.jval.2016.09.1269.
- [14] L. F. Eichenfield *et al.*, “GUIDELINES OF CARE FOR THE MANAGEMENT OF ATOPIC DERMATITIS,” *J Am Acad Dermatol*, vol. 71, no. 1, pp. 116–132, Jul. 2014, doi: 10.1016/j.jaad.2014.03.023.
- [15] J. Leon-Villapalos, M. G. Jeschke, and D. N. Herndon, “Topical management of facial burns,” *Burns*, vol. 34, no. 7, pp. 903–911, Nov. 2008, doi: 10.1016/j.burns.2008.01.025.
- [16] B. Gawronska-Kozak, A. Grabowska, M. Kopcewicz, and A. Kur, “Animal models of skin regeneration,” *Reprod Biol*, vol. 14, no. 1, pp. 61–67, Mar. 2014, doi: 10.1016/j.repbio.2014.01.004.
- [17] “The Principles of Humane Experimental Technique,” *Medical Journal of Australia*, vol. 1, no. 13, pp. 500–500, Mar. 1960, doi: 10.5694/j.1326-5377.1960.tb73127.x.

- [18] “Directive 2010/63/EU of the European Parliament and of the Council of 22 September 2010 on the protection of animals used for scientific purposes (Text with EEA relevance),” <https://webarchive.nationalarchives.gov.uk/eu-exit/https://eur-lex.europa.eu/legal-content/EN/TXT/?uri=CELEX:02010L0063-20190626>. <https://www.legislation.gov.uk/eudr/2010/63> (accessed Oct. 01, 2021).
- [19] R. E. BILLINGHAM and P. B. MEDAWAR, “The Technique of Free Skin Grafting in Mammals,” *Journal of Experimental Biology*, vol. 28, no. 3, pp. 385–402, Sep. 1951, doi: 10.1242/jeb.28.3.385.
- [20] C. E. Wheeler, C. M. Canby, and E. P. Cawley, “Long-Term Tissue Culture of Epithelial-like Cells from Human Skin1,” *Journal of Investigative Dermatology*, vol. 29, no. 5, pp. 383–392, Nov. 1957, doi: 10.1038/jid.1957.114.
- [21] J. G. Rheinwald and H. Green, “Formation of a keratinizing epithelium in culture by a cloned cell line derived from a teratoma,” *Cell*, vol. 6, no. 3, pp. 317–330, Nov. 1975, doi: 10.1016/0092-8674(75)90183-X.
- [22] M. Eisinger, J. S. Lee, J. M. Hefton, Z. Darzynkiewicz, J. W. Chiao, and E. de Harven, “Human epidermal cell cultures: growth and differentiation in the absence of differentiation in the absence of dermal components or medium supplements.,” *Proc Natl Acad Sci U S A*, vol. 76, no. 10, pp. 5340–5344, Oct. 1979.
- [23] Nicholas E. O’Connor, John B. Mulliken, S. Banks-Schlegel, O. Kehinde, and H. Green, “GRAFTING OF BURNS WITH CULTURED EPITHELIUM PREPARED FROM AUTOLOGOUS EPIDERMAL CELLS,” *The Lancet*, vol. 317, no. 8211, pp. 75–78, Jan. 1981, doi: 10.1016/S0140-6736(81)90006-4.
- [24] A. E. Freeman, H. J. Igel, B. J. Herrman, and K. L. Kleinfeld, “Growth and characterization of human skin epithelial cell cultures,” *In Vitro Cell.Dev.Biol.-Plant*, vol. 12, no. 5, pp. 352–362, May 1976, doi: 10.1007/BF02796313.
- [25] J. H. Lillie, D. K. MacCallum, and A. Jepsen, “Fine structure of subcultivated stratified squamous epithelium grown on collagen rafts,” *Exp Cell Res*, vol. 125, no. 1, pp. 153–165, Jan. 1980, doi: 10.1016/0014-4827(80)90199-8.
- [26] E. Bell, B. Ivarsson, and C. Merrill, “Production of a tissue-like structure by contraction of collagen lattices by human fibroblasts of different proliferative potential in vitro.,” *Proc Natl Acad Sci U S A*, vol. 76, no. 3, pp. 1274–1278, Mar. 1979.
- [27] E. Bell, H. P. Ehrlich, D. J. Buttle, and T. Nakatsuji, “Living Tissue Formed in Vitro and Accepted as Skin-Equivalent Tissue of Full Thickness,” *Science*, vol. 211, no. 4486, pp. 1052–1054, Mar. 1981, doi: 10.1126/science.7008197.
- [28] S. Gibbs, S. Murli, G. De Boer, A. Mulder, A. M. Mommaas, and M. Ponc, “Melanosome capping of keratinocytes in pigmented reconstructed epidermis--effect of ultraviolet radiation and 3-isobutyl-1-methyl-xanthine on melanogenesis,” *Pigment Cell Res*, vol. 13, no. 6, pp. 458–466, Dec. 2000, doi: 10.1034/j.1600-0749.2000.130608.x.
- [29] E. H. van den Bogaard *et al.*, “Crosstalk between keratinocytes and T cells in a 3D microenvironment: a model to study inflammatory skin diseases,” *J Invest Dermatol*, vol. 134, no. 3, pp. 719–727, Mar. 2014, doi: 10.1038/jid.2013.417.
- [30] M. Ponc, A. El Ghalbzouri, R. Dijkman, J. Kempenaar, G. van der Pluijm, and P. Koolwijk, “Endothelial network formed with human dermal microvascular endothelial cells in autologous multicellular skin substitutes,” *Angiogenesis*, vol. 7, no. 4, pp. 295–305, 2004, doi: 10.1007/s10456-004-6315-3.
- [31] L. Fusco *et al.*, “Skin irritation potential of graphene-based materials using a non-animal test,” *Nanoscale*, vol. 12, no. 2, pp. 610–622, Jan. 2020, doi: 10.1039/c9nr06815e.
- [32] H. Kandárová *et al.*, “The EpiDerm test protocol for the upcoming ECVAM validation study on in vitro skin irritation tests--an assessment of the performance of the optimised

- test,” *Altern Lab Anim*, vol. 33, no. 4, pp. 351–367, Aug. 2005, doi: 10.1177/026119290503300408.
- [33] S. Sunpreet, *3D Printing in Biomedical Engineering*. Singapore: Springer, 2020.
- [34] C.-J. Bae, A. B. Diggs, and A. Ramachandran, “6 - Quantification and certification of additive manufacturing materials and processes,” in *Additive Manufacturing*, J. Zhang and Y.-G. Jung, Eds. Butterworth-Heinemann, 2018, pp. 181–213. doi: 10.1016/B978-0-12-812155-9.00006-2.
- [35] R. M. Cardoso *et al.*, “Additive-manufactured (3D-printed) electrochemical sensors: A critical review,” *Anal Chim Acta*, vol. 1118, pp. 73–91, Jun. 2020, doi: 10.1016/j.aca.2020.03.028.
- [36] J. K. Placone and A. J. Engler, “Recent Advances in Extrusion-Based 3D Printing for Biomedical Applications,” *Adv Healthc Mater*, vol. 7, no. 8, p. e1701161, Apr. 2018, doi: 10.1002/adhm.201701161.
- [37] M. Van der Walt, T. Crabtree, and C. Albantow, “PLA as a suitable 3D printing thermoplastic for use in external beam radiotherapy,” *Australas Phys Eng Sci Med*, vol. 42, no. 4, pp. 1165–1176, Dec. 2019, doi: 10.1007/s13246-019-00818-6.
- [38] M. S. Lopes, A. L. Jardini, and R. M. Filho, “Poly (Lactic Acid) Production for Tissue Engineering Applications,” *Procedia Engineering*, vol. 42, pp. 1402–1413, Jan. 2012, doi: 10.1016/j.proeng.2012.07.534.
- [39] B. Gupta, N. Revagade, and J. Hilborn, “Poly(lactic acid) fiber: An overview,” *Progress in Polymer Science*, vol. 32, no. 4, pp. 455–482, Apr. 2007, doi: 10.1016/j.progpolymsci.2007.01.005.
- [40] B. E. Grottkau, Z. Hui, C. Ye, and Y. Pang, “3D-printed insert-array and 3D-coculture-array for high-throughput screening of cell migration and application to study molecular and cellular influences,” *Biomed Mater*, vol. 15, no. 5, p. 055028, Aug. 2020, doi: 10.1088/1748-605X/ab98e9.
- [41] K. Li, D. Wang, K. Zhao, K. Song, and J. Liang, “Electrohydrodynamic jet 3D printing of PCL/PVP composite scaffold for cell culture,” *Talanta*, vol. 211, p. 120750, May 2020, doi: 10.1016/j.talanta.2020.120750.
- [42] Z. Jiang, B. Diggle, M. L. Tan, J. Viktorova, C. W. Bennett, and L. A. Connal, “Extrusion 3D Printing of Polymeric Materials with Advanced Properties,” *Adv Sci (Weinh)*, vol. 7, no. 17, p. 2001379, Sep. 2020, doi: 10.1002/advs.202001379.
- [43] C.-Y. Liaw and M. Guvendiren, “Current and emerging applications of 3D printing in medicine,” *Biofabrication*, vol. 9, no. 2, p. 024102, Jun. 2017, doi: 10.1088/1758-5090/aa7279.
- [44] T. Fan and R. Daniels, “Preparation and Characterization of Electrospun Polylactic Acid (PLA) Fiber Loaded with Birch Bark Triterpene Extract for Wound Dressing,” *AAPS PharmSciTech*, vol. 22, no. 6, p. 205, Jul. 2021, doi: 10.1208/s12249-021-02081-z.
- [45] P. Zamiri *et al.*, “The biocompatibility of rapidly degrading polymeric stents in porcine carotid arteries,” *Biomaterials*, vol. 31, no. 31, pp. 7847–7855, Nov. 2010, doi: 10.1016/j.biomaterials.2010.06.057.
- [46] P. E. Haers, R. Suuronen, C. Lindqvist, and H. Sailer, “Biodegradable polylactide plates and screws in orthognathic surgery: technical note,” *J Craniomaxillofac Surg*, vol. 26, no. 2, pp. 87–91, Apr. 1998, doi: 10.1016/s1010-5182(98)80045-0.
- [47] J. M. Holzwarth and P. X. Ma, “Biomimetic nanofibrous scaffolds for bone tissue engineering,” *Biomaterials*, vol. 32, no. 36, pp. 9622–9629, Dec. 2011, doi: 10.1016/j.biomaterials.2011.09.009.
- [48] M. Mohiti-Asli *et al.*, “Ibuprofen loaded PLA nanofibrous scaffolds increase proliferation of human skin cells in vitro and promote healing of full thickness incision

- wounds in vivo,” *J Biomed Mater Res B Appl Biomater*, vol. 105, no. 2, pp. 327–339, Feb. 2017, doi: 10.1002/jbm.b.33520.
- [49] S. Vainionpää, P. Rokkanen, and P. Törmälä, “Surgical applications of biodegradable polymers in human tissues,” *Progress in Polymer Science*, vol. 14, no. 5, pp. 679–716, Jan. 1989, doi: 10.1016/0079-6700(89)90013-0.
- [50] R. M. Rasal, A. V. Janorkar, and D. E. Hirt, “Poly(lactic acid) modifications,” *Progress in Polymer Science*, vol. 35, no. 3, pp. 338–356, Mar. 2010, doi: 10.1016/j.progpolymsci.2009.12.003.
- [51] M. Mizielnińska, U. Kowalska, M. Jarosz, P. Sumińska, N. Landercy, and E. Duquesne, “The Effect of UV Aging on Antimicrobial and Mechanical Properties of PLA Films with Incorporated Zinc Oxide Nanoparticles,” *Int J Environ Res Public Health*, vol. 15, no. 4, p. 794, Apr. 2018, doi: 10.3390/ijerph15040794.
- [52] C. A. Grant, P. C. Twigg, R. Baker, and D. J. Tobin, “Tattoo ink nanoparticles in skin tissue and fibroblasts,” *Beilstein J Nanotechnol*, vol. 6, pp. 1183–1191, May 2015, doi: 10.3762/bjnano.6.120.
- [53] C. Dong and Y. Lv, “Application of Collagen Scaffold in Tissue Engineering: Recent Advances and New Perspectives,” *Polymers (Basel)*, vol. 8, no. 2, p. 42, Feb. 2016, doi: 10.3390/polym8020042.
- [54] S. Ricard-Blum, “The Collagen Family,” *Cold Spring Harb Perspect Biol*, vol. 3, no. 1, p. a004978, Jan. 2011, doi: 10.1101/cshperspect.a004978.
- [55] J. W. Weisel and R. I. Litvinov, “Fibrin Formation, Structure and Properties,” *Subcell Biochem*, vol. 82, pp. 405–456, 2017, doi: 10.1007/978-3-319-49674-0\_13.
- [56] J. W. Weisel, “Fibrinogen and Fibrin,” in *Advances in Protein Chemistry*, vol. 70, Elsevier, 2005, pp. 247–299. doi: 10.1016/S0065-3233(05)70008-5.
- [57] S. A. Sell, M. J. McClure, K. Garg, P. S. Wolfe, and G. L. Bowlin, “Electrospinning of collagen/biopolymers for regenerative medicine and cardiovascular tissue engineering,” *Advanced Drug Delivery Reviews*, vol. 61, no. 12, pp. 1007–1019.
- [58] J. Hwang *et al.*, “Ex Vivo Live Full-Thickness Porcine Skin Model as a Versatile In Vitro Testing Method for Skin Barrier Research,” *Int J Mol Sci*, vol. 22, no. 2, p. 657, Jan. 2021, doi: 10.3390/ijms22020657.
- [59] F. Groeber *et al.*, “A first vascularized skin equivalent as an alternative to animal experimentation,” *ALTEX - Alternatives to animal experimentation*, vol. 33, no. 4, Art. no. 4, Nov. 2016, doi: 10.14573/altex.1604041.
- [60] K. Knoth *et al.*, “Development and evaluation of a quality control system based on transdermal electrical resistance for skin barrier function in vitro,” *Skin Res Technol*, vol. 27, no. 5, pp. 668–675, Sep. 2021, doi: 10.1111/srt.12998.
- [61] S. S. Meisser *et al.*, “Skin barrier damage after exposure to paraphenylenediamine,” *Journal of Allergy and Clinical Immunology*, vol. 145, no. 2, pp. 619-631.e2, Feb. 2020, doi: 10.1016/j.jaci.2019.11.023.
- [62] Y. Kim and K.-M. Lim, “Skin barrier dysfunction and filaggrin,” *Arch Pharm Res*, vol. 44, no. 1, pp. 36–48, Jan. 2021, doi: 10.1007/s12272-021-01305-x.
- [63] Y. Ishitsuka and D. R. Roop, “Loricrin: Past, Present, and Future,” *Int J Mol Sci*, vol. 21, no. 7, p. 2271, Mar. 2020, doi: 10.3390/ijms21072271.
- [64] S. Nithya, T. Radhika, and N. Jeddy, “Loricrin – an overview,” *J Oral Maxillofac Pathol*, vol. 19, no. 1, pp. 64–68, 2015, doi: 10.4103/0973-029X.157204.
- [65] S.-F. Ng, J. J. Rouse, F. D. Sanderson, V. Meidan, and G. M. Eccleston, “Validation of a Static Franz Diffusion Cell System for In Vitro Permeation Studies,” *AAPS PharmSciTech*, vol. 11, no. 3, pp. 1432–1441, Sep. 2010, doi: 10.1208/s12249-010-9522-9.
- [66] P. Ashrafi, Y. Sun, N. Davey, S. C. Wilkinson, and G. P. Moss, “The influence of diffusion cell type and experimental temperature on machine learning models of skin

- permeability,” *J Pharm Pharmacol*, vol. 72, no. 2, pp. 197–208, Feb. 2020, doi: 10.1111/jphp.13203.
- [67] B. C. Sil *et al.*, “3D-printed Franz type diffusion cells,” *Int J Cosmet Sci*, vol. 40, no. 6, pp. 604–609, Dec. 2018, doi: 10.1111/ics.12504.
- [68] A. C. Williams and B. W. Barry, “Penetration enhancers,” *Adv Drug Deliv Rev*, vol. 56, no. 5, pp. 603–618, Mar. 2004, doi: 10.1016/j.addr.2003.10.025.
- [69] D. Işık *et al.*, “Sulfoxide-functionalized nanogels inspired by the skin penetration properties of DMSO,” *Biomater Sci*, vol. 9, no. 3, pp. 712–725, Feb. 2021, doi: 10.1039/d0bm01717e.
- [70] T. Nakamura *et al.*, “Reduction of skin barrier function by proteolytic activity of a recombinant house dust mite major allergen Der f 1,” *J Invest Dermatol*, vol. 126, no. 12, pp. 2719–2723, Dec. 2006, doi: 10.1038/sj.jid.5700584.
- [71] S. Kim *et al.*, “Enhanced Transdermal Delivery by Combined Application of Dissolving Microneedle Patch on Serum-Treated Skin,” *Mol Pharm*, vol. 14, no. 6, pp. 2024–2031, Jun. 2017, doi: 10.1021/acs.molpharmaceut.7b00111.
- [72] R. Wong, S. Geyer, W. Weninger, J.-C. Guimberteau, and J. K. Wong, “The dynamic anatomy and patterning of skin,” *Exp Dermatol*, vol. 25, no. 2, pp. 92–98, Feb. 2016, doi: 10.1111/exd.12832.
- [73] K. Ouwehand, S. W. Spiekstra, T. Waaijman, R. J. Scheper, T. D. de Gruijl, and S. Gibbs, “Technical advance: Langerhans cells derived from a human cell line in a full-thickness skin equivalent undergo allergen-induced maturation and migration,” *J Leukoc Biol*, vol. 90, no. 5, pp. 1027–1033, Nov. 2011, doi: 10.1189/jlb.0610374.
- [74] N. Bechetoille, C. Dezutter-Dambuyant, O. Damour, V. André, I. Orly, and E. Perrier, “Effects of solar ultraviolet radiation on engineered human skin equivalent containing both Langerhans cells and dermal dendritic cells,” *Tissue Eng*, vol. 13, no. 11, pp. 2667–2679, Nov. 2007, doi: 10.1089/ten.2006.0405.
- [75] A. Smith *et al.*, “A Novel Three-Dimensional Skin Disease Model to Assess Macrophage Function in Diabetes,” *Tissue Eng Part C Methods*, vol. 27, no. 2, pp. 49–58, Feb. 2021, doi: 10.1089/ten.TEC.2020.0263.

## List of Figures

- Figure 1 Skin structure** showing the epidermal, dermal, and hypodermal layers and their sublayers. The epidermis is divided into *stratum corneum*, *lucidum*, *granulosum*, *spinosum* and *basale*. The dermis is subdivided into the *papillary* and *reticular layer*. Moreover, cell types of the skin include: keratinocytes, Merkel cells, Langerhans cells, melanocytes, histocytes, fibroblasts, mast cells, and adipocytes are represented. Skin appendages, like hair and glands are also shown. Taken from [3] ..... 6
- Figure 2 Layers of the epidermis.** The epidermis is divided into *stratum corneum*, *lucidum*, *granulosum*, *spinosum* and *basale* (top to bottom). The dermis is implied next to the *stratum basale* harbouring a sensory neuron. Also, a melanocyte and a Merkel cell is represented. The alteration of keratinocytes on their way from the *stratum basale* to the *stratum corneum* is shown here as keratinocytes that turn into cells with lamellar granulae and furthermore into dead cells filled with keratin. Taken from [1] ..... 7
- Figure 3 Types of skin equivalents.** To build 3D skin models keratinocytes can be grown on: (1) a cellular matrix (collagen-fibroblast matrix), (2) an acellular matrix (gel or de-epidermized dermis) or (3) on plasticware or various membranes. After cultivation for several days, the culture medium level is lowered in order to grow the skin equivalents at the air-liquid interface. Days to weeks later, a multilayered stratified epidermis is formed. Created with BioRender.com. .... 11
- Figure 4 Requirements for cell culture inserts:** a practical way to exchange media; sufficient space within the insert for the volume, that is required for the generation of SE; possibility to use different membrane materials; hanging membrane to enable nutrient exchange through both sides of the membrane, compatibility with common cell culture plastic ware. Created with BioRender.com. .... 13
- Figure 5 MTT cell toxicity assay procedure.** The procedure starts with cell seeding on a 96-well plate (1) and subsequent incubation of the plate for 24 hours (2). After the incubation time the treatment media is applied (3). The treated cells are incubated for another 24 hours (4). Afterwards the treatment media is discarded and MTT reagent is applied (5). MTT reagent is then reduced to coloured formazan crystals (6). This change in colour can be measured at a wavelength of 570 nm (7). Created with BioRender.com..... 17

**Figure 6 First construction version of 3D printed inserts.** On the left side the bottom part, with a round stand area and a central zylinder is shown. The clinder has seven windows and on the upper part, a saving for the cap, which is depicted on the right side. Both fit together perfectly and form a snap closure, in the middle of which any membrane can be clamped. The cells that subsequently form the SE are cultivated on the membrane. Depending on the print size, the insert can be placed in a standard 6-well plate or 12-well plate..... 21

**Figure 7 Second construction version of 3D printed inserts.** This graphic shows an adapted construction version of the bottom section of an insert in 12-well plate size. The cylinder has been decentralized and the number of windows has been reduced from seven to four. .... 22

**Figure 8 Third construction version of 3D printed inserts.** Here, an adapted construction version of the bottom section of an insert in 12-well plate size in shown. The windows were enlarged to let out air that could accumulate under the membrane. .... 23

**Figure 9 Fourth construction version of 3D printed inserts.** Here, an adapted construction version of the bottom section of an insert in 12-well plate size is shown. The windows were enlarged to let out air that could accumulate under the membrane. Furthermore, a phase has been added to the upper edge of the lower part and the upper part, creating a groove, which makes it easier to remove the upper part from the lower part in order to harvest the SE. The cylinder was also moved a more into the center of the stand area to make the side window more accessible to the media. .... 24

**Figure 10 Fifth construction version of 3D printed inserts.** Both parts of the inserts were improved in this construction step. In order to increase the inner filling volume of the inserts, the membrane support surface was placed further down. Furthermore, the snap closure extends over almost the entire surface of the upper part. .... 25

**Figure 11 Final construction version of 3D printed inserts.** Bottom (left) and top (right) part construction of the insert is shown. The bottom part consists out of a round stand area and a decentralized zylinder with four windows. The windows reach the membran area, which is directly on the border of the snap closure. The snap closure connects bottom and upper part. The top part has an increased filling volume compared to the first versions of the construction. .... 26

**Figure 12 Twist lock construction.** Bottom (left) and upper (right) part of a insert with twist lock is shown in this render graphic..... 27

**Figure 13 Final construction of 3D printed inserts together with the permeability ring.** From left to right: construction of the bottom section of the insert, which can be connected via a snap closure to the top part of the insert. After the generation of SE on the insert membrane, the permeability ring can be pushed into the top part of the insert. This clamps the SE, excludes edge effects, and standardizes the assay through a defined area..... 28

**Figure 14 Nanoparticle tracking analysis (NTA) of polylactic acid (PLA) printing filament after an incubation period of 24 hours.** PLA pellets were incubated at 37 °C after either no sterilization treatment, rinsing with ethanol (EtOH) or rinsing with EtOH and subsequent UV irradiation. These were compared to filtered PBS (fPBS) without any exposure to PLA. Treated groups did not exhibit signs of nanoparticle release compared to fPBS. Pellets without sterilization treatment released a significant concentration [particle/ml] of nanoparticles compared to all other groups. n = 9 in PBS group n = 27 in treatment groups, \*\* P ≤ 0.01, \*\*\* P ≤ 0.001 ..... 30

**Figure 15 Hematoxylin and eosin (HE) staining of pilot experiments on full thickness skin equivalents (SE) generated in 3D printed.** The epidermis (purple) on top of the collagen matrix harboring few fibroblasts (light pink). The membrane material (transparent) was not removed for the histological analysis. Cultured on a 3D printed 12-well plate insert is depicted. Harvested on ALI day 10, seeded with a concentration of  $3 \cdot 10^4$  fibroblasts/ml in a collagen matrix on a polycarbonate membrane. SE showed the formation of an epidermis and dermis, albeit lacking the defined stratified layers of differentiated keratinocytes. In both cases only a few fibroblasts can be seen in the dermis..... 31

**Figure 16 Hematoxylin and eosin (HE) staining of pilot experiments on full thickness skin equivalents (SE) generated in commercial inserts.** The epidermis (purple) on top of the collagen matrix harboring few fibroblasts (light pink). The membrane material (transparent) was not removed for the histological analysis. SE, generated on a 6-well plate bought insert. Seeding number of  $1 \cdot 10^5$  fibroblasts/ml in a collagen matrix on a polyethyleneterephthalat (PET) membrane. SE showed the formation of an epidermis and dermis, albeit lacking the defined stratified layers of differentiated keratinocytes. Like in SE, cultured on a 3D printed insert only a few fibroblasts can be seen in the dermis..... 31

**Figure 17 Visual assessment of cell confluency, as well as morphology of fibroblast monolayers cultured under different media conditions.** Investigation of monolayers cultured in keratinocyte and fibroblast specific growth media, as well

as a 1:1 mix of both media for a period of 19 days at 37 °C, 5 % CO<sub>2</sub> and moderate humidity. Pictures were taken on days 1, 5, 9, 14, and 19. Fibroblasts exhibited less proliferation in keratinocyte specific growth media. n=8..... 33

**Figure 18 Thiazolyl blue tetrazolium bromide (MTT) assay of fibroblast and keratinocytes monolayers cultured under different media conditions.**

Investigation of monolayers cultured in keratinocyte and fibroblast specific growth media, as well as a 1:1 mix of both media for 5 days at 37 °C, 5 % CO<sub>2</sub> and moderate humidity. Fibroblasts exhibited less viability in keratinocyte specific growth media. In contrast keratinocytes had the highest viability under these conditions. n=2..... 34

**Figure 19 Hematoxylin and eosin (HE) staining of full thickness skin equivalents (SE) on day 14 compared to day 19 on air liquid interface (ALI) testing different seeding parameters.**

All SE were cultured on commercial 6-well plate size insert and the keratinocytes, forming the epidermis, were seeded immediately after hydrogel polymerization. A & D: fibroblast seeding concentration of 1 · 10<sup>5</sup> fibroblasts/ml in a collagen matrix. B & E: fibroblast seeding concentration of 5 · 10<sup>5</sup> fibroblasts/ml in a collagen matrix. C & F: fibroblast seeding concentration of 1 · 10<sup>5</sup> fibroblasts/ml in a fibrin-collagen matrix. Epidermis (purple) on top of a fibroblasts (fibrin-) collagen matrix (light pink) on membrane material (transparent bottom layer)..... 35

**Figure 20 Pilot tests of skin barrier assay with a 3D printed permeability ring using fluorescent measurements of Alexa Fluor<sup>®</sup> and Riboflavin/DMSO.**

Left: Intact skin barrier was provided with Alexa Fluor<sup>®</sup>. Right: Skin barrier was irritated with DMSO, and permeability was tested with riboflavin. In contrast to the intact SE, an almost linear increase in fluorescence can be seen. Measurements were taken at different timepoints from zero minutes to two hours. Furthermore, PBS as well as the highest possible concentration of fluorophores (Alexa Fluor<sup>®</sup>: 10 mg/ml, riboflavin: 1 mM) was measured. Fluorescence was measured at 584 nm (reference 620 nm) for Alexa Fluor<sup>®</sup> and 485 nm (reference 520 nm) for riboflavin. .... 37

**Figure 21 Franz diffusion cell.**

Perfusion material or dye is applied to the donor compartment and detected in the receptor compartment after passing the membrane or sample material. The receiver solution is mixed with a stirrer. Samples selection takes place via a sampling port. Taken from [66] ..... 41

## List of Tables

<b>Table 1 Final printing parameters.</b> In the columns the parameter name, the associated units and final values are listed.....	14
--	----

## List of Abbreviation

Abbreviation	Meaning
3D	Tri-dimensional
ALI	Air-liquid interface
BPE	Bovine Pituitary Extract
DMEM	Dulbecco's Modified Eagle Medium
DMSO	Dimethyl sulfoxide
Ethanol	EtOH
FDM	Fused deposition modelling
FLM	Fused layer modelling
fPBS	Filtered PBS
HBSS	Hank's Balanced Salt Solution
HE	Hematoxylin and eosin
MTT	thiazolyl blue tetrazolium bromide
PET	Polyethyleneterephthalat
PPT	Photopolymerization techniques
SB	Skin barrier
SE	Skin equivalent
SLS	Selective laser sintering
UV	Ultraviolet